

PLM-Net: Perception Latency Mitigation Network for Vision-Based Lateral Control of Autonomous Vehicles

Aws Khalil , and Jaerock Kwon , *Senior Member, IEEE*

Abstract—This study introduces the Perception Latency Mitigation Network (PLM-Net), a novel deep learning approach for addressing *perception latency* in vision-based Autonomous Vehicle (AV) lateral control systems. *Perception latency* is the delay between capturing the environment through vision sensors (e.g., cameras) and applying an action (e.g., steering). This issue is understudied in both classical and neural-network-based control methods. Reducing this latency with powerful GPUs and FPGAs is possible but impractical for automotive platforms. PLM-Net consists of two models: the Base Model (BM) and the Timed Action Prediction Model (TAPM). BM represents the original Lane Keeping Assist (LKA) system, while TAPM predicts future actions for different latency values. By integrating these models, PLM-Net mitigates perception latency. The final output is determined through linear interpolation of BM and TAPM outputs based on real-time latency. This design addresses both constant and varying latency, improving driving trajectories and steering control. Experimental results validate the efficacy of PLM-Net across various latency conditions. Source code: <https://github.com/AwsKhalil/oscar/tree/devel-plm-net>.

Index Terms—Autonomous Vehicle Navigation, Deep Learning in Robotics and Automation, Model Learning for Control, Learning from Demonstration

I. INTRODUCTION

A. Motivation

Vision-based Autonomous Vehicle (AV) control functions in a similar way to how the human brain interprets and responds to visual information. Both share the same perception-planning-control (sense-think-act) cycle. In this cycle, there is a latency between sensing the environment and applying a corresponding action, which makes the human reaction time always higher than zero [1]. Similarly, it is challenging to completely eliminate this latency in AV control [2], and reducing it through powerful GPUs and FPGAs is impractical in automotive platforms. This latency, if not properly mitigated, can result in a number of issues, ranging from trivial ones like uncomfortable rides to serious ones like endangering the safety of the passengers. Therefore, the ability of an AV driving system to effectively mitigate latency is crucial for ensuring safety. We hypothesize that the human brain have internal mechanisms such as anticipating or predicting future actions to mitigate the latency [3]. Inspired by this, we propose a deep neural network architecture with similar predictive capabilities.

A. Khalil and J. Kwon are with the University of Michigan-Dearborn, Michigan, 48128 USA.(e-mail: awskh@umich.edu, jrkwon@umich.edu).

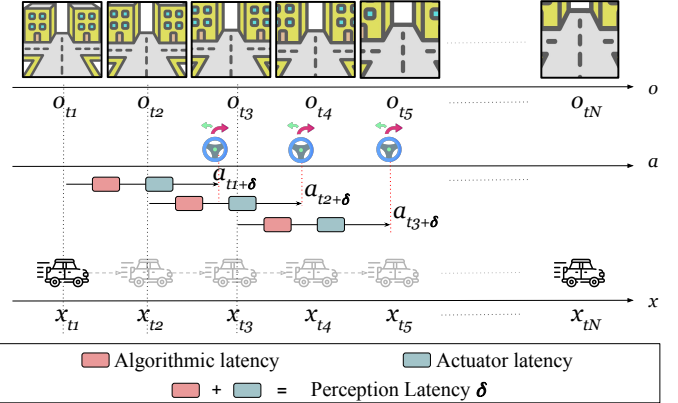


Fig. 1. Perception Latency definition. When vehicle state is x_t and we have observation o_t , the corresponding action a_t is applied at time $t + \delta$ not t ($o_t \rightarrow a_{t+\delta}$). By the time this action is applied, the vehicle state has changed and we have a new observation. The perception latency has two components: the algorithmic latency, and the actuator latency.

In this paper, we refer to this latency as the *perception latency* δ , as shown in Fig.1. When vehicle state is x_t and we have observation o_t , the corresponding action a_t is applied at time $t + \delta$ rather than at time t ($o_t \rightarrow a_{t+\delta}$). By the time this action is applied, the vehicle state has changed and we have a new observation. The *perception latency* has two components: the algorithmic latency, which is the time required for the algorithm to infer an action from an observation, and the actuator latency, which is the time required to apply the inferred action. The actuator latency, known as steering lag in lateral control [4], can be considered constant [4]. However, as mentioned in [5], the high processing cost of visual algorithms leads to uneven time delays based on the driving scenario, which leads to an overall *perception latency* that is time-varying.

To address both constant and time-varying *perception latency* encountered during lane keeping, we propose a deep-learning-based approach, focusing primarily on vision-based AV lateral control. The contribution of this paper will be discussed after explaining the effect of the *perception latency* on AV lateral control.

B. Latency Effect on AV Lateral Control

Vision-based AV lateral control for lane keeping can be achieved using various methods. The traditional approach

involves incorporating a computer vision module for lane-marking detection alongside a classical control module for path planning and control. Alternatively, a deep-learning-based approach, such as imitation learning [6], directly maps visual input to control actions, like steering angle. This paper adopts the latter method.

The effect of *perception latency* on AV lateral control during lane keeping is highly dependent on vehicle speed. At low speeds, the scene does not change significantly between the time the vehicle receives the observation at time t and the time it applies the action at time $t + \delta$, because the traveled distance during the latency period is minimal ($d = \delta v$). In this scenario, it is reasonable to assume that $a_t \approx a_{t+\delta}$, making the effect of δ negligible. Thus, at low speeds, we can consider that at time t , the action a_t corresponding to observation o_t is applied immediately ($o_t \rightarrow a_t$).

The effect of latency on AV control during lane keeping is illustrated in Fig. 2. Two vehicles drive at a constant low speed: the green vehicle uses the normal real-time observation, assuming zero latency, while the red vehicle uses the delayed observation, mimicking the *perception latency* effect. Both vehicles start from position A and move towards position D . If we timestamp each position, then $t_A < t_B < t_C < t_D$. For the green vehicle at position B , the available observation is o_{t_B} and the corresponding action is a_{t_B} . For the red vehicle at the same position, the available observation is $o_{t_B-\delta}$ and the corresponding action is $a_{t_B-\delta}$. This pattern continues for the other positions. Both vehicles remain in their lanes at positions A and B , before encountering any curves, because they started within the lane and continued straight where the steering angle is zero. Thus, at positions A and B , the actions a_t and $a_{t-\delta}$ are effectively the same. At position C , the first curve is encountered. The green vehicle successfully turns left to stay in the lane, but the red vehicle continues straight. This deviation occurs because the red vehicle's input observation at position C is $o_{t_C-\delta}$, not o_{t_C} , leading it to apply the action $a_{t_C-\delta}$ at position C . After this first curve, the red vehicle's zigzag trajectory becomes difficult to correct, even on a straight road, due to the incorrect action taken at position C , which causes subsequent incorrect observations.

In this approach, to mitigate the perception latency and avoid this unstable driving behavior, the main objective would be to predict the correct action from the delayed observation input.

C. Contribution

We introduce the Perception Latency Mitigation Network (*PLM-Net*), outlined in Fig. 3. This novel deep learning approach is intended to work easily and without requiring any changes to the original vision-based LKA system of the AV. As depicted in Fig. 3, *PLM-Net* leverages a Timed Action Prediction Model (*TAPM*) alongside the Base Model (*BM*), where the latter represents the preexisting vision-based LKA system. The design of the *TAPM* is inspired by our prior work, *ANEC* [7], and the Branched Conditional Imitation Learning model (*BCIL*) proposed by Codevilla et al. [8]. It combines the concept of a predictive model capable of forecasting future

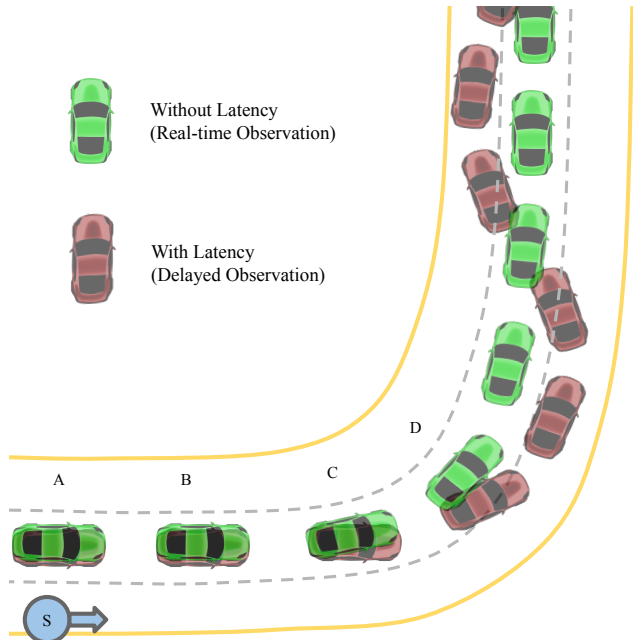


Fig. 2. Illustration of Perception Latency Effect on Lateral Control During Lane Keeping. The green vehicle exhibits driving behavior with real-time observations, while the red vehicle demonstrates driving behavior with a delayed observation input. Both vehicles maintain a constant low speed. Motion starts at position A . Positions A and B depict both vehicles driving straight, staying within their lanes, with minimal steering adjustments ($a_{t_A} \approx a_{t_B} \approx 0.0$). At position C , where the first curve is encountered, the green vehicle successfully adjusts its trajectory by turning left to stay in the lane, while the red vehicle continues straight due to the delayed observation input. Subsequently, the red vehicle struggles to recover from its zigzag-shaped trajectory, highlighting the impact of incorrect actions on subsequent observations.

action from current visual observation, akin to *ANEC* [7] (originally inspired by the human driver capability of dealing with the perception latency [9]), with the notion of employing multiple sub-models within the *BCIL* framework [8] to provide different predictive action values corresponding to different latency levels. Additionally, similar to the ‘command’ input used in *BCIL* to select a submodel, the real-time *perception latency* δ_t is used to determine the final action value. The final action value \tilde{a}_t^{PLM} is determined through the function $f(\tilde{a}_t, \delta_t)$ where it performs linear interpolation based on the real-time latency value δ_t given all the predictive action values provided by the *TAPM* (\tilde{a}_t^{TAPM}) and the current action value provided by the *BM* (\tilde{a}_t^{BM}). A comprehensive explanation of our proposed method is provided in Section III.

The structure of this paper proceeds as follows: Section II presents an overview of related research, while Section III outlines the proposed methodology. Following this, Section IV and Section V present the experimental setup and the experimental findings within the simulation environment, accompanied by a comprehensive analysis. Finally, Section VI summarizes the core findings of the study and provides valuable insights into potential avenues for future research.

II. RELATED WORK

In the domain of vision-based control, the issue of *perception latency* remains significantly understudied across both

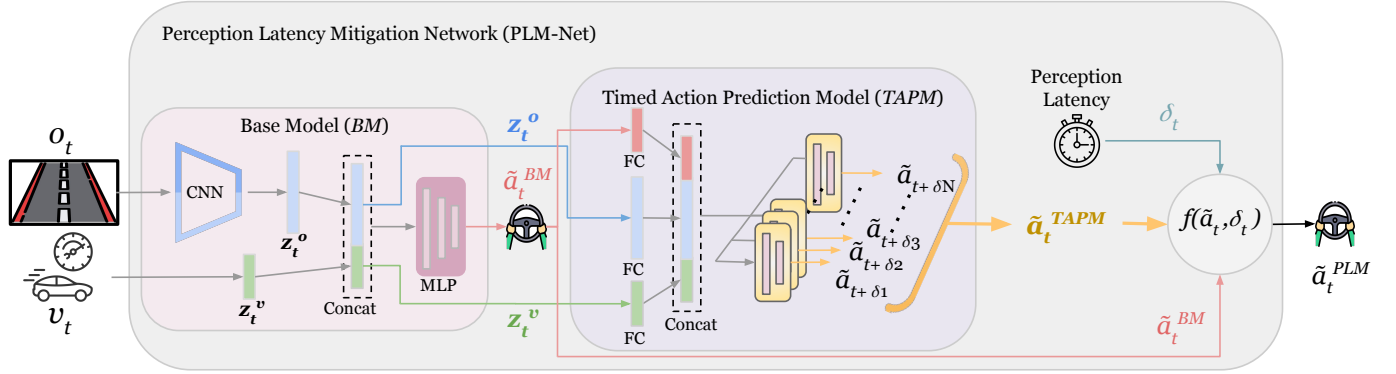


Fig. 3. Overview of the Perception Latency Mitigation Network (*PLM-Net*). By leveraging a Timed Action Prediction Model (*TAPM*) alongside the Base Model (*BM*), *PLM-Net* enhances the system's ability to mitigate perception latency. The *TAPM* incorporates predictive modeling to anticipate future actions based on current visual observations. Additionally, the integration of multiple sub-models within the framework enables adaptation to varying latency levels, as the final action value \tilde{a}_t^{PLM} is determined through the function $f(\tilde{a}_t, \delta_t)$ where it performs linear interpolation based on the real-time latency value δ_t given all the predictive action values provided by the *TAPM* (\tilde{a}_t^{TAPM}) and the current action value provided by the *BM* (\tilde{a}_t^{BM}). See Section III for detailed explanation.

classical control models, and neural-network-based control models. In classical control methods, discussions surrounding latency in autonomous driving have largely revolved around computational delays associated with hardware deployment [10]–[13] and communication delays related to network performance [14]–[19]. To the best of our knowledge, only two studies within the classical control domain have attempted to address aspects of *perception latency*, such as time-variant latency, input delay, or steering lag [4], [5]. However, these discussions primarily centered on classical-control-based solutions. On the other hand, within vision-based neural network control models, research efforts have primarily concentrated on model development, largely neglecting the *perception latency* issue [6], [20]–[26]. Only few studies have discussed the *perception latency* [2], [7], [27]–[29].

Li et al. [2] underscored the significance of addressing latency in online vision-based perception systems. To tackle this issue, they introduced a methodology for assessing the real-time performance of perception systems, effectively balancing accuracy and latency. However, it is important to note that the paper primarily focuses on proposing a metric and benchmark for evaluating the real-time performance of perception systems, rather than offering a direct solution for vehicle control. While their approach provides valuable insights into quantifying the trade-off between accuracy and latency in perception systems, it does not directly address the challenges associated with mitigating latency in autonomous driving scenarios. Our previous work [7], addressed the *perception latency* issue by proposing the *Adaptive Neural Ensemble Controller (ANEC)*. However, *ANEC* assumed *perception latency* to be constant and did not address time-varying latency. Weighted sum was used to combine the output from the two driving models, but the weight function parameters had to be carefully chosen and adjusted by hand. This makes it hard to replicate in different environments as you need to optimize these parameters for each new environment. Mao et al. [27] explored latency in the context of video object detection by analyzing the detection latency of various video object detectors. While they introduced

a metric to quantify latency, their study focused on measurement rather than proposing solutions to mitigate latency. Kocic et al. [28] tried to decrease the latency in driving by altering the neural network architecture. Although this approach could potentially diminish latency, preserving the original accuracy poses a significant challenge. Wu et al. [29] emphasized that control-based driving models, which convert images into control signals, inherently exhibit *perception latency* and are susceptible to failure due to their focus on the current time step. In response, they developed Trajectory-guided Control Prediction (TCP), a multi-task learning system integrating a control prediction model with a trajectory planning model. However, this approach necessitates the extraction of precise trajectories, presenting a notable challenge.

In our approach, we acknowledge the inevitability of latency and strive to minimize its impact by intelligently integrating predicted future actions with the current action based on the real-time latency value. This combination mechanism allows our proposed method to effectively mitigate the latency, ensuring better performance in vision-based autonomous vehicle lateral control systems.

III. METHOD

This section outlines the comprehensive approach undertaken to develop and evaluate the Perception Latency Mitigation Network (*PLM-Net*). The section is divided into four key subsections. First, we introduce the proposed *PLM-Net*, detailing the conceptual framework and the rationale behind its design. Second, we delve into the architecture of the *PLM-Net* models, providing an in-depth analysis of the structural components and their interconnections. Third, we describe the training process of the *PLM-Net* models. Finally, we present the performance metrics used to evaluate the efficacy of the *PLM-Net*, highlighting the criteria and benchmarks for assessing its ability to mitigate perception latency in vision-based autonomous vehicle control systems.

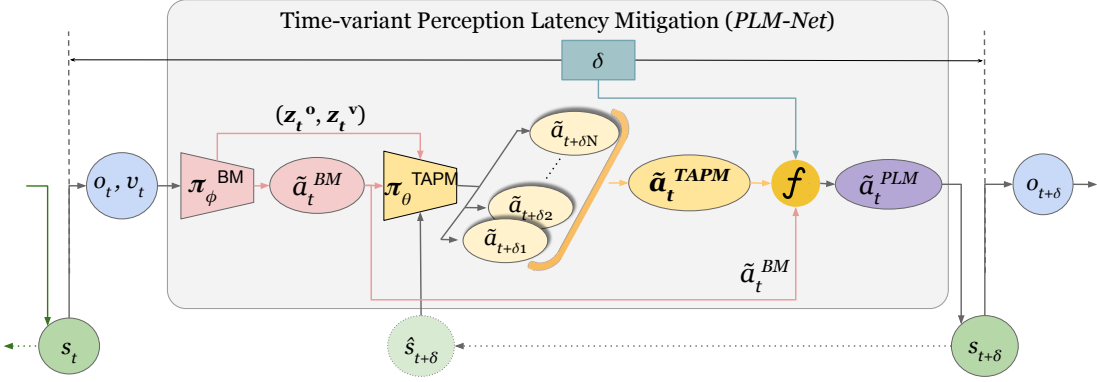


Fig. 4. PLM-Net Diagram. This diagram illustrates the operation of the two models within the *PLM-Net* architecture in mitigating perception latency. The Base Model (*BM*), governed by policy π_ϕ^{BM} , processes visual observations o_t and vehicle speed v_t to generate action \tilde{a}_t , as described in Eq. (1). Meanwhile, the Timed Action Prediction Model (*TAPM*), guided by policy π_θ^{TAPM} , generates different predictive action values based on different latency values. Each action corresponding to a specific future state (e.g., $\tilde{a}_{t+\delta_1}$ for state $s_{t+\delta_1}$), as detailed in Eq. (2). The inputs to π_θ^{TAPM} include the output of π_ϕ^{BM} (i.e., \tilde{a}_t) along with image feature vector z_t^o and vehicle velocity vector z_t^v . Subsequently, linear interpolation, as described in Algorithm 1, combines the outputs of π_ϕ^{BM} and π_θ^{TAPM} based on the real-time perception latency δ to yield the final action of the *PLM-Net*.

A. Proposed Network PLM-Net

As shown in Fig.3, the *PLM-Net* has two major components, Base Model (*BM*) and Timed Action Prediction Model (*TAPM*). This novel deep learning approach smoothly integrates the *TAPM* with the original vision-based LKA system of the AV, represented by the *BM*. Fig.4 shows how these two models mitigate the *perception latency* where π_ϕ^{BM} is the *BM* policy and π_θ^{TAPM} is the *TAPM* policy. As explained in (1), given the vehicle state s_t at time t , π_ϕ^{BM} takes the input $i_t = \{o_t, v_t\}$ where o_t is the visual observation and v_t is the vehicle speed at time t and provides the action \tilde{a}_t^{BM} .

$$\tilde{a}_t^{BM} = \pi_\phi^{BM}(i_t) = \pi_\phi^{BM}(o_t, v_t). \quad (1)$$

The *TAPM* is a predictive model, meaning it can estimate the future state $\hat{s}_{t+\delta}$ of the vehicle. The policy π_θ^{TAPM} generates a set of predictive action values \tilde{a}_t^{TAPM} , where each action corresponds to a future state at a specific latency value in δ^{TAPM} .

The number of predictive actions in the vector \tilde{a}_t^{TAPM} , depends on the number of submodels in *TAPM*. If there are N submodels, then $\delta^{TAPM} = [\delta_1, \delta_2, \dots, \delta_N]$. For example, if $\delta_1 = 0.15$ seconds, then the action $\tilde{a}_{t+0.15}$ represents the action that the *BM* would take if the vehicle was in the state $s_{t+0.15}$. The process of obtaining the vector \tilde{a}_t^{TAPM} is described by (2), where the inputs to π_θ^{TAPM} are the output of the π_ϕ^{BM} (i.e., the action \tilde{a}_t^{BM}) along with two feature vectors; the image feature vector z_t^o and the vehicle velocity vector z_t^v , both derived from π_ϕ^{BM} .

$$\begin{aligned} \tilde{a}_t^{TAPM} &= [\tilde{a}_{t+\delta_1}, \tilde{a}_{t+\delta_2}, \dots, \tilde{a}_{t+\delta_N}] \\ &= \pi_\theta^{TAPM}(\tilde{a}_t, z_t^o, z_t^v). \end{aligned} \quad (2)$$

The final action of the *PLM-Net* \tilde{a}_t^{PLM} is obtained through linear interpolation, as explained in Algorithm 1. This interpolation uses the output of both π_ϕ^{BM} and π_θ^{TAPM} based on the real-time *perception latency* value δ . Since \tilde{a}_t^{BM} represents the current action value without latency mitigation, it is equivalent

Algorithm 1 Linear Interpolation for Latency

Require: δ, δ_{ref} // Target latency value and list of known latency.
Require: $a_{\delta_{ref}}$ // Corresponding action values for known latency.
Ensure: a_δ // Interpolated action value for target latency

- 1: **for** $j = 1$ to N **do**
- 2: **if** $\delta_{ref}[j] < \delta < \delta_{ref}[j + 1]$ **then**
- 3: $a_\delta \leftarrow a_{\delta_{ref}}[j] + \frac{\delta - \delta_{ref}[j]}{\delta_{ref}[j+1] - \delta_{ref}[j]} \times (a_{\delta_{ref}}[j + 1] - a_{\delta_{ref}}[j])$
- 4: **end if**
- 5: **end for**
- 6: **return** a_δ

to $\tilde{a}_{t+0.0}$, so we add the value 0.0 to δ^{TAPM} and the action \tilde{a}_t^{BM} to \tilde{a}_t^{TAPM} to form δ_{ref} and \tilde{a}_{ref} , respectively, as shown in (3).

$$\begin{aligned} \delta_{ref} &= [0.0, \delta^{TAPM}] = [0.0, \delta_1, \delta_2, \dots, \delta_N], \\ \tilde{a}_{\delta_{ref}} &= [\tilde{a}_t^{BM}, \tilde{a}_t^{TAPM}] \\ &= [\tilde{a}_{t+0.0}, \tilde{a}_{t+\delta_1}, \tilde{a}_{t+\delta_2}, \dots, \tilde{a}_{t+\delta_N}]. \end{aligned} \quad (3)$$

This makes the *PLM-Net* capable of mitigating both constant and time-variant *perception latency* δ .

B. PLM-Net Models Architecture

The architecture of *PLM-Net* models is illustrated in Fig. 5. The network design of *BM* is presented in Fig. 5(a), and the network design of *TAPM* is presented in Fig. 5(b).

The *BM* network design is inspired by the NVIDIA PilotNet structure [30] with modifications tailored to our requirements. Specifically, we adapt the network to accept visual observations (o_t) and vehicle speed (v_t) as inputs and to predict steering angle (action \tilde{a}_t^{BM}) as output, and we add dropout layers to improve generalization and avoid overfitting. The *BM* features two primary inputs: the visual observation o_t and the vehicle speed v_t . The visual observation undergoes processing through five convolutional layers, then a flatten layer to obtain the image feature vector z_t^o . Simultaneously, the vehicle speed input is directed through a fully-connected layer that has 144

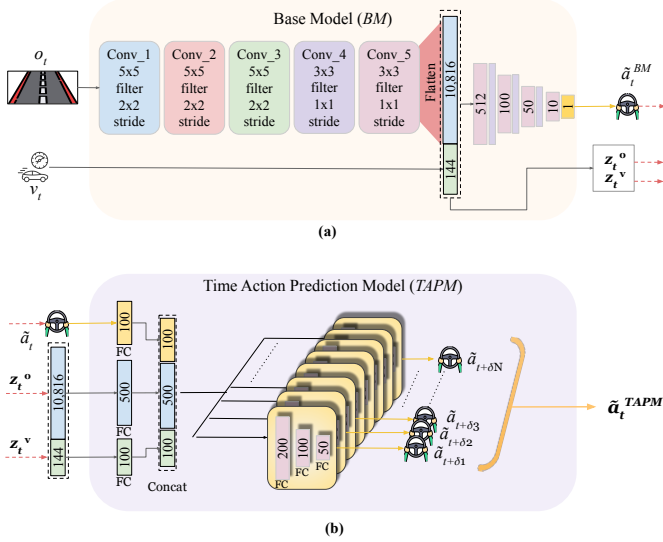


Fig. 5. PLM-Net Architecture. (a) The *BM* network design, inspired by the NVIDIA PilotNet structure [30], processes visual observation o_t and vehicle speed v_t to predict steering angle \tilde{a}_t^{BM} . It utilizes five convolutional layers and a multi-layer perceptron network with dropout layers, including fully-connected layers with neuron counts of 512, 100, 50, and 10. (b) The *TAPM* network design, inspired by ANEC [7] and BCIL [8], processes inputs forwarded by the *BM* (\tilde{a}_t^{BM} , z_t^o , z_t^v) through fully-connected layers with a 100, 500, and 100 neurons, respectively. These layers are then concatenated and forwarded to sub-models, including fully connected layers with neuron counts of 200, 100, and 50, and dropout layers with a rate of 0.3. Each submodel will provide distinct future action for a certain latency value. The outputs of the submodels forms the *TAPM* output \tilde{a}_t^{TAPM} , which is a set of predictive action values corresponding to distinct latency values.

neurons, resulting in the formation of the vehicle speed vector z_t^v . Subsequently, the image feature vector z_t^o and the vehicle speed vector z_t^v are concatenated and forwarded to a multi-layer perceptron (MLP) network. This MLP configuration consists of four fully-connected layers interspersed with three dropout layers. The fully-connected layers contain 512, 100, 50, and 10 neurons, respectively. The dropout layers maintains a dropout rate of 0.3. The final output of the *BM* \tilde{a}_t^{BM} , the image feature vector z_t^o , and the vehicle speed vector z_t^v , are forwarded to the *TAPM* network.

The *TAPM* network design is the result of fusing two key ideas. Firstly, it incorporates a predictive model, similar to ANEC [7], which was inspired by human drivers' ability to mitigate perception latency. Secondly, it utilizes the BCIL framework [8], employing multiple sub-models to provide a range of predictive action values that align with different latency levels, and adding a 'command' input, representing the *perception latency* δ , to influence the final action value. The *TAPM* network inputs are \tilde{a}_t^{BM} , z_t^o , and z_t^v , forwarded from the *BM*. These three inputs goes to a 100-neuron, 500-neuron, and 100-neuron fully-connected layers, respectively. The outputs of these three layers are then concatenated to be forwarded to all sub-models. Each sub-model consist of three fully connected layers, with 200, 100, and 50 neurons, interspersed with two dropout layers with a dropout rate of 0.3. The sub-models outputs will result in \tilde{a}_t^{TAPM} shown in (2).

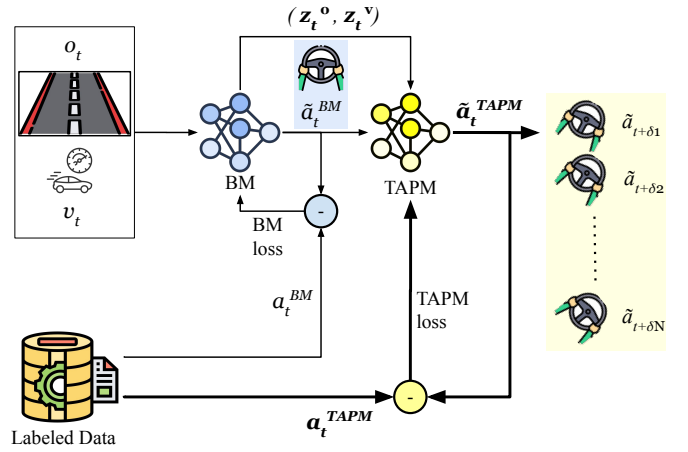


Fig. 6. The training process for *PLM-Net* models. Initially, the *BM* policy π_ϕ^{BM} is trained using supervised learning on dataset D , optimizing parameters ϕ to minimize prediction error (Eq. (4)). Subsequently, a new dataset D^{TAPM} is generated from D to train the *TAPM* policy π_θ^{TAPM} , optimizing parameters θ to minimize error between predicted and ground truth future actions (Eq. (5)). During *TAPM* training, the *BM* remains non-trainable to ensure *TAPM* reliance on its output. Input data pass through the *BM*, generating output action \tilde{a}_t^{BM} and input vectors z_t^o and z_t^v , which feed into the *TAPM*. The *TAPM* utilizes these inputs to generate future action values (\tilde{a}_t^{TAPM}).

C. PLM-Net Models Training

The functionality of a vision-based *LKA* system, can be achieved through imitation learning where we directly map the steering angle (i.e., action a_t) to the input $i_t = \{o_t, v_t\}$ where o_t is the visual observation and v_t is the vehicle speed at time t . The training dataset collected by an expert driver can be defined as $D = \{i_t, a_t\}_{t=1}^M$, where M is the total time-steps. Fig. 6, explains the training process of the *PLM-Net* models. Learning the *BM* policy π_ϕ^{BM} is a supervised learning problem. The parameters ϕ of the policy is optimized by minimizing the prediction error of a_t given the input i_t , as shown in (4), where we use the Mean Squared Error (MSE) to calculate the loss per sample. Once optimized, the *BM* can predict the action \tilde{a}_t^{BM} given the input $i_t = \{o_t, v_t\}$ at time t as shown in (1).

$$\arg \min_{\phi} \frac{1}{N} \sum_{t=1}^N (\tilde{a}_t^{BM} - a_t)^2 \quad (4)$$

To learn the *TAPM* policy π_θ^{TAPM} , we generate a new dataset D^{TAPM} from the original dataset D , mapping the input $i_t = \{o_t, v_t\}$ to a N distinct future actions a_t^{TAPM} corresponding to N distinct latency values δ^{TAPM} (2), where

$$D^{TAPM} = \{i_t, a_t^{TAPM}\}_{t=1}^M = \{i_t, [a_{t+\delta_1}, \dots, a_{t+\delta_N}]\}_{t=1}^M \quad (2)$$

The optimization of the parameters θ of the *TAPM* policy π_θ^{TAPM} , is explained in (5). We minimize the prediction error of a_t^{TAPM} given the input i_t , where a_t^{TAPM} is the ground truth values of \tilde{a}_t^{TAPM} . We use MSE to calculate the loss per sample.

$$\arg \min_{\theta} \frac{1}{M} \sum_{t=1}^M \sum_{j=1}^N (\tilde{a}_{t+\delta_j} - a_{t+\delta_j})^2 \quad (5)$$

To integrate *TAPM* with the existing *LKA* system without modifying it, we set the *BM* to be non-trainable during the training of the *TAPM* to make sure that the *TAPM* depends on the output of the *BM*.

D. Performance Metrics

In the context of lateral control for AVs, *perception latency* can lead to delayed or incorrect actions, particularly affecting the steering angle, which in turn impacts the overall trajectory of the vehicle as explained in Section I-B. Therefore, to assess *PLM-Net*'s ability to mitigate this latency, two primary evaluation criteria can be employed: steering angle accuracy and trajectory similarity. Accurate steering is essential for maintaining lane position and following the desired path, ensuring precise vehicle control even under latency conditions. Meanwhile, trajectory similarity evaluates how closely the vehicle's path adheres to the intended trajectory, providing insight into the broader impact of *perception latency* on vehicle navigation and the efficacy of *PLM-Net* in mitigating it.

IV. EXPERIMENTAL SETUP

This section outlines the experimental setup for validating the Perception Latency Mitigation Network (*PLM-Net*). We begin by describing the simulator used for creating a controlled testing environment. Next, we detail the dataset for training and evaluation. We then discuss the methods for measuring driving performance, followed by the parameter tuning process. After that, an ablation study is presented to highlight key development decisions. Finally, we specify the computational environment and machine learning framework, including hardware and software configurations.

A. Simulator

Our experiments were carried out using the OSCAR simulator [31], renowned for its user-friendly interface and customizable features. OSCAR operates on ROS (Robotic Operating System) [32], seamlessly integrated with the Gazebo multi-robot 3D simulator [33]. Specifically, we utilized ROS Melodic and Gazebo 9 for our experiments.

B. Dataset

a) Training and Test Tracks: The track used to train the *PLM-Net* is the same training track used in our prior work [7]. To evaluate the *PLM-Net* ability to mitigate the *perception latency*, we designed a new three-lane test track that has several turns in left and right directions and straight road segments, as shown in Fig. 7.

b) Data Collection: Our training dataset, denoted as *D*, was collected by a human driver navigating the training track using OSCAR simulator. This simulator captures visual observations via a mounted camera on the vehicle, alongside critical control values such as steering angle, throttle position, braking pressure, time, velocity, acceleration, and position. High-quality data was collected using the Logitech G920 dual-motor feedback driving force racing wheel with pedals and a gear shifter, resulting in approximately 115,000 clean training

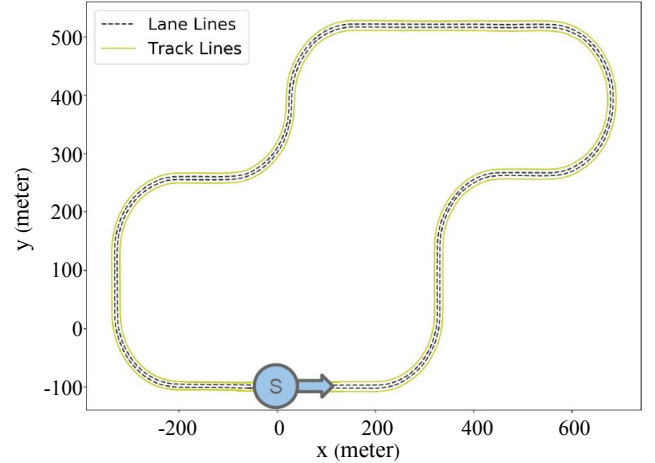


Fig. 7. Test track used for evaluating the *PLM-Net* performance. The track features a combination of straight sections and curves to simulate real-world driving conditions. The starting point is marked as *S* and the arrow indicates the driving direction. This track was chosen to test the vehicle's ability to maintain lane keeping and handle perception latency during both straight and curved segments.

TABLE I
STEERING AND VELOCITY STATISTICS

	Steering	Velocity
Mean	-0.003923	20.310327
Std	0.176994	2.924156
Min	-1.000000	0.018407
25%	-0.069025	18.301480
50%	0.000000	19.883244
75%	0.058849	22.329700
Max	0.691892	29.936879

samples. Table I provides detailed statistics on the steering and velocity data.

The steering angle for the vehicle is represented on a scale from -1 to 1 , where 0 denotes the center position. According to the right-hand rule, positive steering angles (0 to 1) correspond to rotations to the left, and negative steering angles (0 to -1) correspond to rotations to the right. The steering wheel has a maximum rotation angle of $\pm 450^\circ$. This mapping implies that a steering angle of 1 corresponds to a 450° rotation to the left, while a steering angle of -1 corresponds to a 450° rotation to the right. Thus, the steering angle range is scaled such that 0 to 1 maps to 0° to 450° and 0 to -1 maps to 0° to -450° .

c) Data Balancing: As shown in Table I, around 50% of the steering values in our dataset approximately equates to 0.0 , indicating the vehicle traveling on a straight road segment. Training a driving model solely on this dataset would introduce bias. To address this, we conducted histogram-based data balancing to reduce the skew towards zero steering values. Fig. 8 illustrates the steering angle histogram before (left) and after (right) the balancing process. Post-balancing, our dataset comprised approximately 67,000 data samples.

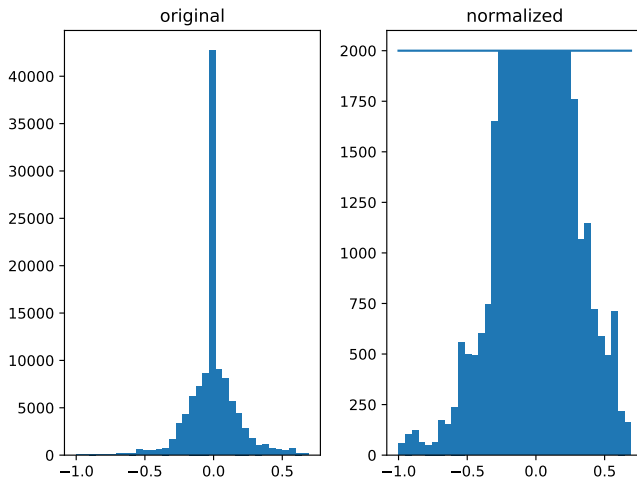


Fig. 8. Histogram-based data balancing based on steering angle values. The left image shows the steering histogram before data balancing and the right image shows the histogram after balancing.

d) Data Augmentation: To improve the model’s generalization capabilities and augment dataset diversity during training, we implemented data augmentation techniques. Each image presented to the network undergoes a random subset of transformations, including horizontal flipping, where the steering value is negated, and random changes in brightness, while preserving the original steering angle. These augmentation techniques have proven effective in enhancing the robustness of our model during training.

C. Driving Performance Evaluation

While Section III-D explained the rationale behind choosing the performance metrics and their importance, this section discusses the adopted methods to measure them in our experiments.

a) Steering Angle Accuracy: We analyzed the steering angle values under different conditions: *BM* driving without latency, *BM* driving with latency but without *TAPM*, and *BM* driving with latency and *TAPM* (utilizing *PLM-Net*). This analysis is conducted both qualitatively, through visual inspection, and quantitatively, by calculating metrics such as Mean Absolute Error (MAE), Mean Squared Error (MSE), and Root Mean Squared Error (RMSE).

b) Trajectory Similarity: The performance metrics used to compare the driving trajectories were adopted from [34] and [35]. We measure the similarity between driving trajectories based on lane center positioning. We use partial curve mapping, Frechet distance, area between curves, curve length, and dynamic time warping from [34], and the Driving Trajectory Stability Index (DTSI) from [35].

D. Parameter Tuning

For the *TAPM*, we used $N = 5$ submodels, meaning the *TAPM* predicts five future actions for five different latency values in δ^{TAPM} . Specifically, the latency values starts with $\delta_1 = 0.15$ seconds, with increments of 0.05 seconds, resulting

TABLE II
NUMBER OF TRAINABLE AND NON-TRAINABLE PARAMETERS FOR BOTH *BM* AND *TAPM* MODELS.

	Total Parameters	Trainable Parameters	Non-trainable Parameters
<i>BM</i>	5,874,566	5,874,566	0
<i>TAPM</i>	12,256,396	6,250,205	6,006,191

in $\delta^{TAPM} = [0.15, 0.20, 0.25, 0.30, 0.35]$ seconds. Consequently, the predictive action vector \tilde{a}_t^{TAPM} in (2) becomes:

$$\tilde{a}_t^{TAPM} = [\tilde{a}_{t+0.15}, \tilde{a}_{t+0.20}, \tilde{a}_{t+0.25}, \tilde{a}_{t+0.30}, \tilde{a}_{t+0.35}]$$

As detailed in (3), the reference latency vector δ_{ref} and the corresponding action vector $\tilde{a}_{\delta_{ref}}$ are formed by including the *BM* action for zero latency. Thus, δ_{ref} and $\tilde{a}_{\delta_{ref}}$ become:

$$\delta_{ref} = [0.0, 0.15, 0.20, 0.25, 0.30, 0.35].$$

$$\tilde{a}_{\delta_{ref}} = [\tilde{a}_{t+0.0}, \tilde{a}_{t+0.15}, \tilde{a}_{t+0.20}, \tilde{a}_{t+0.25}, \tilde{a}_{t+0.30}, \tilde{a}_{t+0.35}]$$

These configurations enable the *PLM-Net* to handle both constant and time-varying perception latency within the range $[0 - 0.35]$ seconds.

Both models, *BM* and *TAPM*, were trained using the Adam optimizer [36] with a batch size of 32 and a learning rate of 0.001. Table II, shows the number of trainable and non-trainable parameters for the *BM* and the *TAPM*. The *BM* has 6,006,191 parameters, in which all of them are trainable. The *TAPM* has 12,256,396 total parameters, where 6,250,205 are trainable and 6,006,191 are non-trainable since the *BM* layers are set to be not trainable when training the *TAPM*. For the performance metric *DTSI*, we used the default parameters recommended in [35].

E. Ablation Study

In our exploration of different model architectures for the *TAPM* network, we experimented with various configurations to optimize performance. Initially, we introduced an additional fully-connected layer with 500 neurons after the concatenation layer preceding the five sub-models. However, this adjustment overly complicated the learning process for the predictive action values. Since this layer was shared among all sub-models, it hindered their individual learning capacities, resulting in subpar outcomes. Further experimentation involved modifying the number of layers within the sub-models. Reducing the layers to two, with 100 and 50 neurons respectively, led to the model’s inability to effectively learn predictive actions. Similarly, adding an extra fully-connected layer to each sub-model with 300 neurons yielded comparable (if not slightly inferior) results to the existing architecture, thus introducing unnecessary complexity without significant improvement. Additionally, we explored the integration of Long Short-Term Memory (LSTM) [37] layers into the sub-models to capture temporal information. However, this approach encountered substantial challenges. Firstly, the model’s complexity increased significantly, impeding computational efficiency. Secondly, the nature of capturing temporal information hindered conventional data balancing techniques and

TABLE III

STEERING ANGLE ERROR METRICS. COMPARISON OF STEERING ANGLE ERROR BETWEEN *BM* DRIVING WITHOUT LATENCY, *BM* DRIVING WITH LATENCY OF 0.2 SECONDS, AND *PLM-Net* DRIVING WITH THE SAME LATENCY

<i>BM</i> , No latency vs.	MAE ↓	MSE ↓	RMSE ↓
<i>BM</i> , Latency = 0.2 sec	0.1915	0.0716	0.2676
<i>PLM-Net</i> , Latency = 0.2 sec	0.0726	0.0125	0.1119

random data sampling from the dataset to enhance batch diversity.

During model training, we found that a batch size of 32 yielded optimal results compared to smaller sizes such as 16 and 8. Furthermore, we experimented with adjusting the learning rate from 0.001 to 0.0001. However, the model failed to converge under the lower learning rate, suggesting that the original rate was more conducive to effective training.

F. Computational Environment and Machine Learning Framework

Our machine learning framework is built upon TensorFlow and Keras libraries. Specifically, we utilized Keras version 2.2.5 in conjunction with TensorFlow-GPU version 1.12.0, leveraging CUDA 9 and cuDNN 7.1.2 for GPU acceleration. All computational experiments were conducted on a hardware setup featuring an Intel i7 – 10700K CPU, 32GB of RAM, and an NVIDIA GeForce RTX 2080 with 8GB of GPU memory. The operating system employed for these experiments was Ubuntu 18.04.6.

V. EXPERIMENTAL RESULTS

Our experimental design aimed to investigate the impact of *perception latency* on driving and assess the efficacy of our proposed solution, *PLM-Net*, in mitigating this effect (as detailed in Section I-B). To simulate latency, we introduced delays in the input data and apply closed-loop velocity control to make the vehicle drive at a constant speed (around 60 km/h), mimicking real-world scenarios where perception and decision-making processes are delayed. For instance, with a 0.2-second latency, the available visual observation at time t becomes $o_{t-0.2}$ instead of o_t , causing the baseline model (*BM*) to generate delayed actions $\tilde{a}_{t-0.2}^{BM}$, which *PLM-Net* aims to correct to \tilde{a}_t .

We assess the impact of *perception latency* through a comparison of driving behaviors: *BM* without latency, *BM* with latency, and *PLM-Net* with latency. Successful mitigation by *PLM-Net* is indicated when its driving performance closely resembles that of the latency-free *BM*. Our evaluation involves analyzing steering angle accuracy and driving trajectory similarity, as detailed in Section IV-C, for both constant and time-variant *perception latency*.

A. Constant Perception Latency Mitigation

In evaluating *PLM-Net* under constant *perception latency*, we focus on a latency of 0.2 seconds, with similar trends

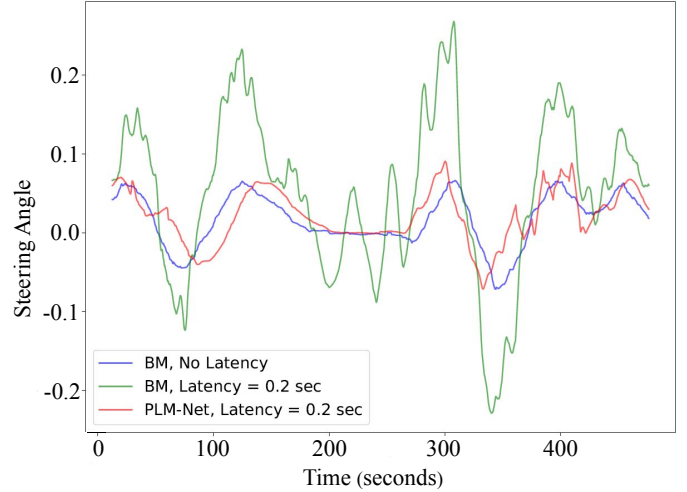


Fig. 9. Qualitative comparison of steering angle over time. The blue line represent the *BM* driving on the test track with no latency. The green line represent the *BM* driving on the test track with 0.2 seconds latency. The red line the *PLM-Net* driving on the test track with the same latency value.

observed for other constant latency values, as illustrated in Appendix A. Fig.9 provides a qualitative comparison of steering angles over time between *BM* with and without latency and *PLM-Net* with the same latency. In this figure, the blue line represents *BM* driving without latency, the green line represents *BM* driving with 0.2 seconds latency, and the red line represents *PLM-Net* driving with 0.2 seconds latency. Additionally, Fig.10 provides a visual representation of vehicle trajectories on the test track, colored based on steering angle, to further elucidate the comparative performance. Table III quantifies steering angle errors, demonstrating *PLM-Net*'s superior performance in reducing errors compared to *BM* under identical latency conditions. Under a constant *perception latency* of 0.2 seconds, the performance of the *BM* significantly decreased. The Mean Absolute Error (MAE) between the *BM* without latency and the *BM* with latency is 0.1915, indicating a substantial degradation in steering angle accuracy. However, when using *PLM-Net*, the performance decline was mitigated, with the MAE reduced to 0.0726. This represents a 62.1% improvement in MAE compared to the *BM* under the same latency condition. Additionally, the Mean Squared Error (MSE) and Root Mean Squared Error (RMSE) were similarly improved with *PLM-Net*, showing reductions of 82.5% and 58.2%, respectively.

Furthermore, Fig.11 presents trajectory comparisons qualitatively, while Table IV presents trajectory comparisons quantitatively, showing *PLM-Net*'s ability to maintain accurate driving trajectories despite latency-induced challenges. Each color-coded trajectory corresponds to a different driving condition: blue for *BM* driving without latency, green for *BM* driving with 0.2 seconds latency, and red for *PLM-Net* driving with 0.2 seconds latency. Examining the deviation from the lane center on the full track, the Partial Curve Mapping metric for *BM* with 0.2 seconds latency increased by 238.7%, while *PLM-Net* maintained a much smaller increase of only 11.1%. Similarly, improvements in Frechet distance, area between

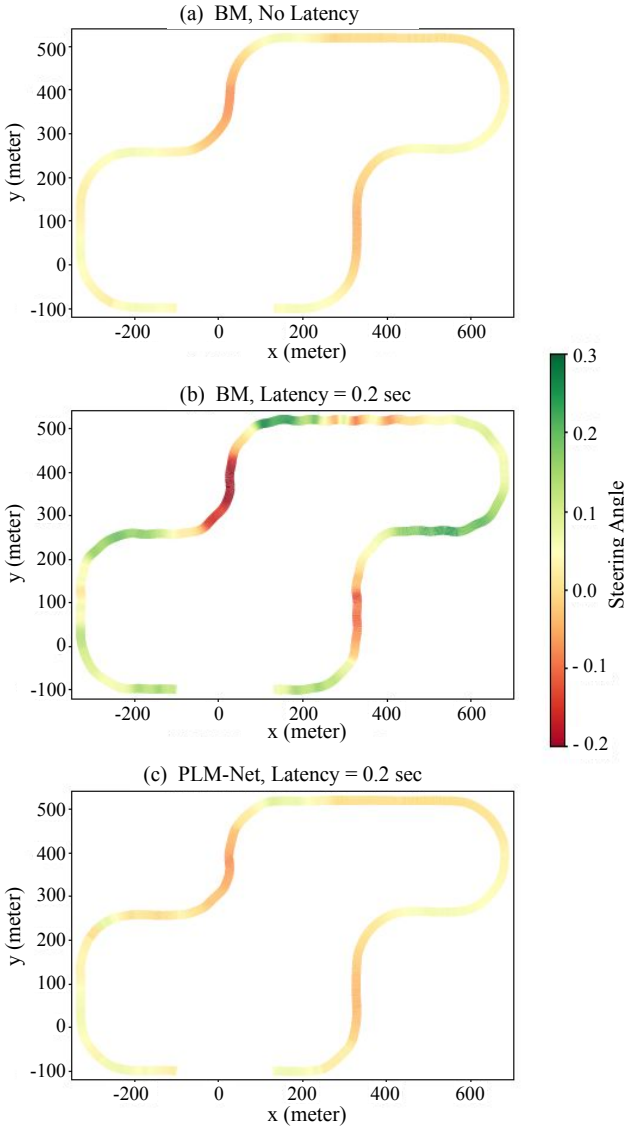


Fig. 10. Vehicle trajectories colored by steering angle. (a) The trajectory of the *BM* driving with no latency. (b) The trajectory of the *BM* driving with 0.2 seconds latency. (c) The trajectory of the *PLM-Net* driving with 0.2 seconds latency.

curves, curve length, and DTSI demonstrate that *PLM-Net* significantly reduces the trajectory deviation caused by latency. The additional segments of Fig.11 and Table IV, specifically parts (b), (c), and (d), which depict the trajectories on a straight road, right turn, and left turn, respectively, also demonstrate that *PLM-Net* effectively mitigates latency, similar to the results observed on the full track.

B. Time-variant Perception Latency Mitigation

For time-variant *perception latency*, we evaluate *PLM-Net* against varying latency levels ([0.0 – 0.35] seconds). Similar to the constant latency scenario, the upper image in Fig.12 illustrates qualitative steering angle comparisons over time, with the blue line representing *BM* driving without latency, the green line representing *BM* driving with time-variant latency,

and the red line representing *PLM-Net* driving with time-variant latency. The lower image illustrates the varying latency values experienced by both models over time. Additionally, Fig.13 provides a visual representation of vehicle trajectories on the test track, colored based on steering angle values. Table V quantifies steering angle errors, demonstrating *PLM-Net*'s effectiveness in reducing errors compared to *BM* under time-variant latency conditions. Under a time-variant *perception latency* of [0 – 0.35] seconds, the performance of the Base Model (*BM*) significantly decreased. The Mean Absolute Error (MAE) between the *BM* without latency and the *BM* with latency is 0.3336, indicating a substantial degradation in steering angle accuracy. However, when using *PLM-Net*, the performance decline was mitigated, with the MAE reduced to 0.0710. This represents a 78.7% improvement in MAE compared to the *BM* under the same latency condition. Additionally, the Mean Squared Error (MSE) and Root Mean Squared Error (RMSE) were similarly improved with *PLM-Net*, showing reductions of 94.2% and 76.0%, respectively.

Fig.14 presents trajectory comparisons qualitatively, while Table VI presents trajectory comparisons quantitatively, confirming *PLM-Net*'s successful mitigation of time-variant *perception latency*. Each color-coded trajectory corresponds to a different driving condition: blue for *BM* driving without latency, green for *BM* driving with time-variant latency, and red for *PLM-Net* driving with time-variant latency. The Partial Curve Mapping metric revealed a 396.6% increase in deviation from the lane center for *BM* with [0.0 – 0.35] seconds time-variant latency on the full track, while *PLM-Net* showed a more modest increase of 114.0%. Similarly, the Frechet distance for *BM* increased by 254.9%, compared to a 66.2% increase for *PLM-Net*. This pattern of reduced deviation is also reflected in the improvements in area between curves, curve length, and DTSI, indicating that *PLM-Net* significantly mitigates the trajectory deviations caused by latency. Parts (b), (c), and (d) of Fig.14 and Table VI, which illustrate the trajectories during a straight segment, a right turn, and a left turn, respectively, exhibit results consistent with the full track, confirming that *PLM-Net* successfully mitigates latency.

Overall, the experimental findings underscore *PLM-Net*'s robustness in mitigating both constant and time-variant *perception latency*, indicating its potential for enhancing driving performance in real-world scenarios.

VI. CONCLUSION

In this paper, we proposed and evaluated *PLM-Net*, a novel approach to mitigate perception latency in vision-based lateral control systems for autonomous vehicles. By incorporating a Timed Action Predictive Model (*TAPM*) alongside a Base Model (*BM*), our system anticipates and adjusts for latency, enhancing stability and safety in lateral control. This predictive capability allows *PLM-Net* to maintain more accurate control even with time-varying latencies.

Our approach leverages deep learning to predict future actions based on current observations and vehicle speed, providing a more responsive control system. The *TAPM* was trained to predict a series of future actions. Interpolation

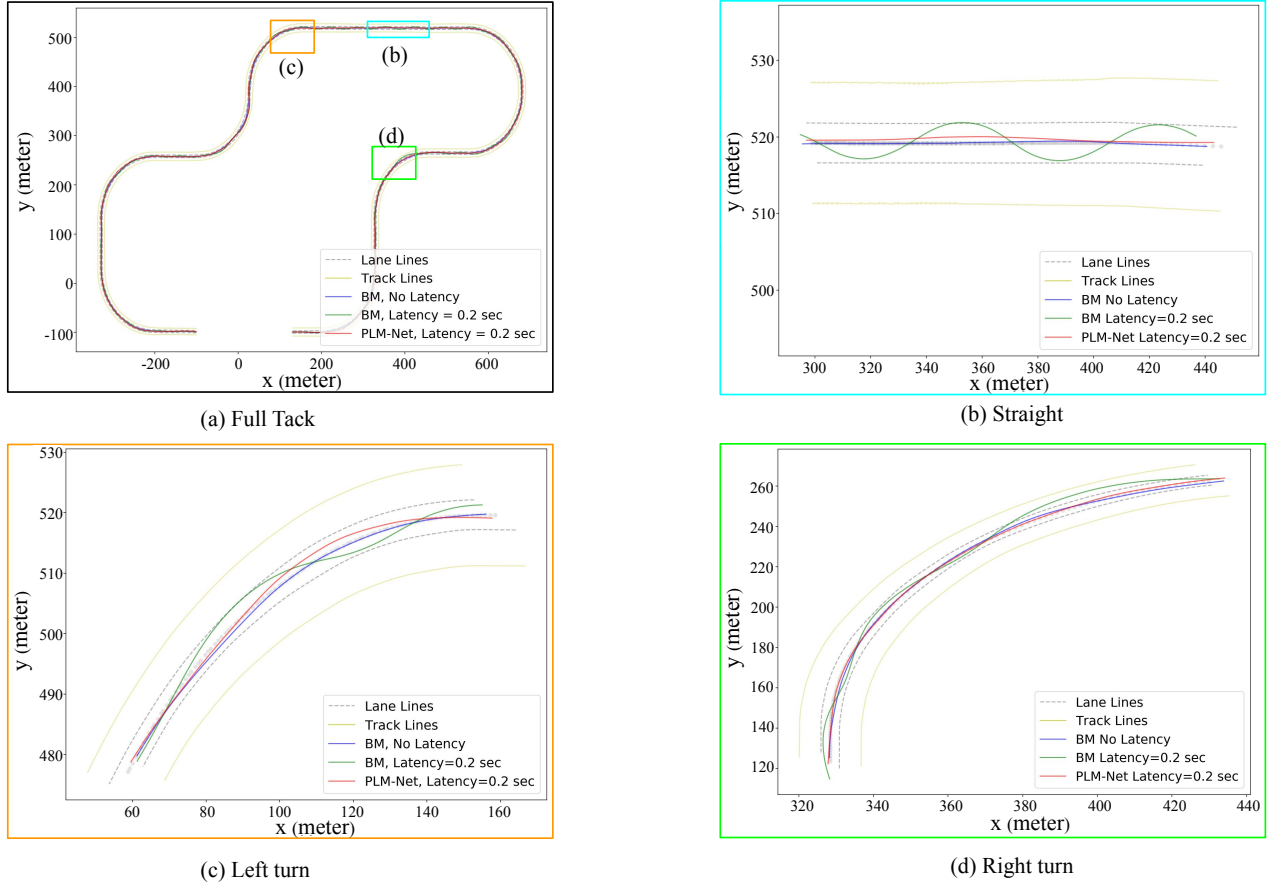


Fig. 11. Qualitative comparison of trajectories on test track. Comparison of driving trajectories on the test track, highlighting differences between: The *BM* driving with no latency (blue line), the *BM* driving with with 0.2 seconds latency (green line), and the *PLM-Net* driving with 0.2 seconds latency (red line). (a) The trajectories on the full test track. (b) The trajectories on a straight road segment. (c) The trajectories on a left turn. (d) The trajectories on a right turn.

TABLE IV

QUANTITATIVE COMPARISON OF DRIVING TRAJECTORY SIMILARITY, BETWEEN *BM* DRIVING WITHOUT LATENCY, *BM* DRIVING WITH LATENCY OF 0.2 SECONDS, AND *PLM-Net* DRIVING WITH THE SAME LATENCY. ALL DRIVING MODELS' TRAJECTORIES ARE COMPARED WITH THE LANE CENTER ON FULL TRACK, STRAIGHT ROAD, LEFT TURN, AND RIGHT TURN.

Fig.11 ref.	Driving Model	Partial	Frechet	Area	Curve	Dynamic	$\overline{DTSL} \downarrow$
		Curve \downarrow Mapping	Distance \downarrow	Between \downarrow Curves	Length \downarrow	Time \downarrow Warping	
(a) Full Track	BM, No Latency (ref)	1.19	2.176	4658.15	0.349	1253.21	0.034
(a) Full Track	BM, Latency = 0.2 sec	4.03	5.469	23045.1	0.767	2594.39	0.072
(a) Full Track	PLM-Net, Latency = 0.2 sec	1.322	3.418	39523.2	0.374	2299.84	0.036
(b) Straight	BM, No Latency (ref)	24.475	5.095	13.556	0.077	76.376	0.012
(b) Straight	BM, Latency = 0.2 sec	351.807	9.048	227.119	0.209	338.861	0.095
(b) Straight	PLM-Net, Latency = 0.2 sec	137.353	6.117	66.545	0.093	136.861	0.016
(c) Left turn	BM, No Latency (ref)	0.895	3.966	41.402	0.178	67.892	0.025
(c) Left turn	BM, Latency = 0.2 sec	1.3	5.405	141.041	0.234	156.02	0.048
(c) Left turn	PLM-Net, Latency = 0.2 sec	0.674	1.5	71.816	0.05	81.885	0.01
(d) Right turn	BM, No Latency (ref)	0.293	1.546	90.228	0.048	79.036	0.037
(d) Right turn	BM, Latency = 0.2 sec	0.927	5.357	384.746	0.124	232.834	0.055
(d) Right turn	PLM-Net, Latency = 0.2 sec	0.745	2.863	45.779	0.063	69.018	0.078

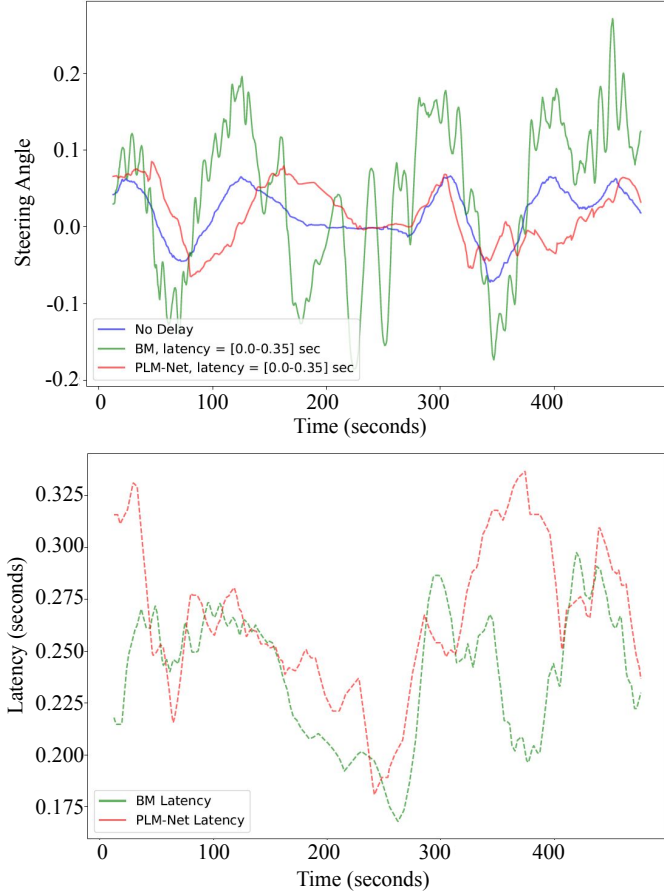


Fig. 12. Qualitative comparison of steering angle over time is depicted in the upper image. The blue line represents the *BM* driving without latency on the test track. Meanwhile, the green line illustrates *BM*'s performance under time-variant latency, ranging from 0.0 to 0.35 seconds. The red line showcases the *PLM-Net*'s driving behavior under the same time-variant latency conditions. In the lower image, latency values against time are presented. The green line corresponds to the latency experienced by the *BM*, while the red line represents the latency encountered by the *PLM-Net*.

TABLE V

COMPARISON OF STEERING ANGLE ERROR BETWEEN *BM* DRIVING WITH NO LATENCY AND WITH TIME-VARIANT LATENCY [0.0 – 0.35] SECONDS, AND *PLM-NET* DRIVING WITH THE SAME TIME-VARIANT LATENCY

<i>BM</i> , No latency vs.	MAE ↓	MSE ↓	RMSE ↓
<i>BM</i> , Latency = [0.0 – 0.35] sec	0.3336	0.1871	0.4326
<i>PLM-Net</i> , Latency = [0.0 – 0.35] sec	0.0710	0.0108	0.1037

is then used on these actions and the action predicted by the original LKA system (i.e., *BM*) based on the real-time perception latency to provide the *PLM-Net* final output.

Through comprehensive experimentation, we demonstrated the effectiveness of *PLM-Net* in reducing the negative impacts of latency across varying levels, such as steering angle errors and unstable driving trajectories.

Future research could focus on enhancing the robustness of *PLM-Net* in diverse real-world environments, investigating its scalability to handle more complex driving scenarios, and exploring additional techniques to further optimize its performance and efficiency.

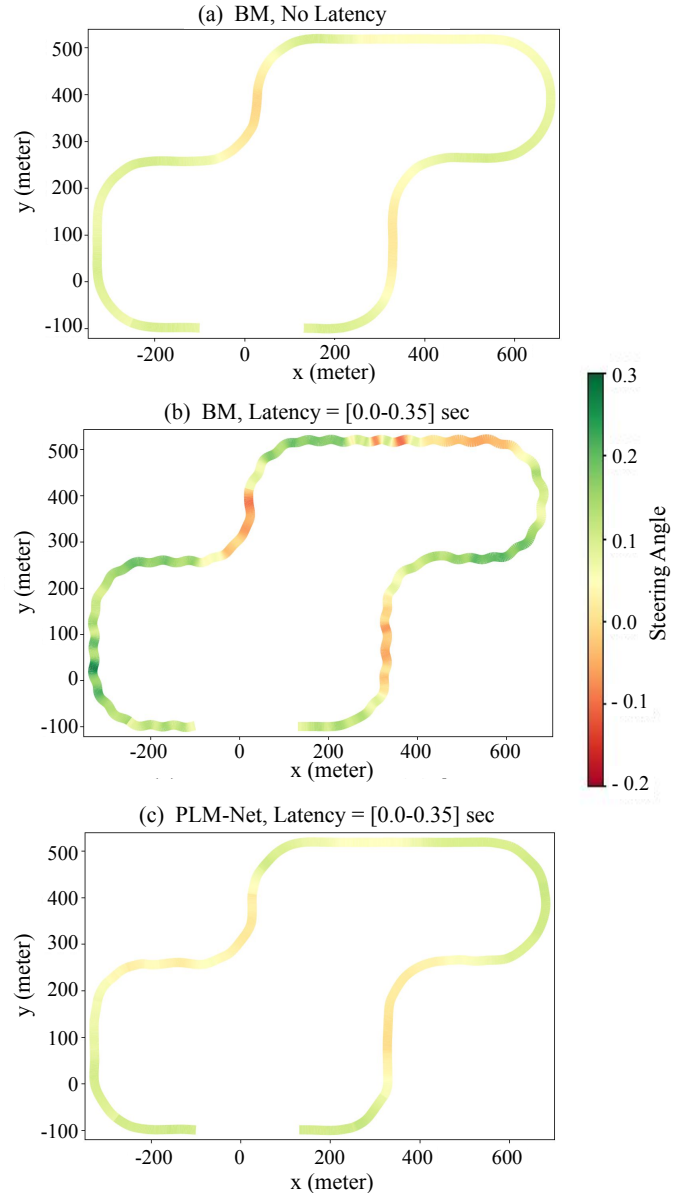


Fig. 13. Colored trajectories based on steering angle. (a) The trajectory of the *BM* driving with no latency. (b) The trajectory of the *BM* driving under time-variant latency [0.0 – 0.35] seconds. (c) The trajectory of the *PLM-Net* driving under time-variant latency [0.0 – 0.35] seconds.

REFERENCES

- [1] J. Kwon and Y. Choe, "Enhanced facilitatory neuronal dynamics for delay compensation," in *2007 International Joint Conference on Neural Networks*. IEEE, 2007, pp. 2040–2045.
- [2] M. Li, Y.-X. Wang, and D. Ramanan, "Towards streaming perception," in *European Conference on Computer Vision*. Springer, 2020, pp. 473–488.
- [3] M. K. Ho and T. L. Griffiths, "Cognitive science as a source of forward and inverse models of human decisions for robotics and control," *Annual Review of Control, Robotics, and Autonomous Systems*, vol. 5, pp. 33–53, 2022.
- [4] S. Xu, H. Peng, and Y. Tang, "Preview path tracking control with delay compensation for autonomous vehicles," *IEEE Transactions on Intelligent Transportation Systems*, vol. 22, no. 5, pp. 2979–2989, 2020.
- [5] Q. Liu, Y. Liu, C. Liu, B. Chen, W. Zhang, L. Li, and X. Ji, "Hierarchical lateral control scheme for autonomous vehicle with uneven time delays induced by vision sensors," *Sensors*, vol. 18, no. 8, p. 2544, 2018.

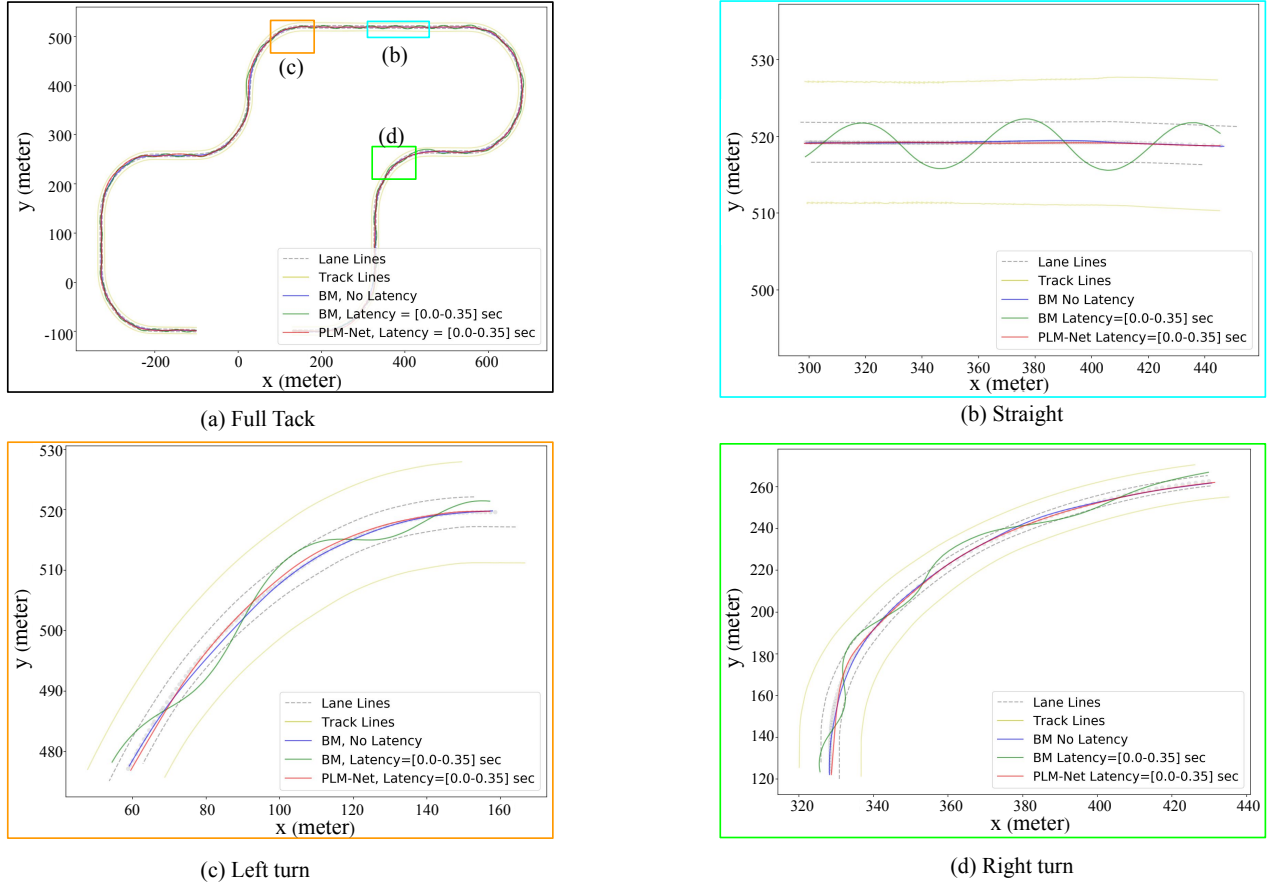


Fig. 14. Trajectory comparison between: The *BM* driving with no latency (blue line), the *BM* driving with time-variant latency [0.0 – 0.35] seconds (green line), and the *PLM-Net* driving within the same time-variant latency range [0.0 – 0.35] seconds. (a) The trajectories on the full test track. (b) The trajectories on a straight road segment. (c) The trajectories on a left turn. (d) The trajectories on a right turn.

TABLE VI

COMPARATIVE ANALYSIS OF DRIVING TRAJECTORY SIMILARITY. *BM* DRIVING WITHOUT LATENCY, *BM* DRIVING UNDER TIME-VARIANT LATENCY RANGING FROM 0.0 TO 0.35 SECONDS, AND *PLM-Net* DRIVING WITHIN THE SAME TIME-VARIANT LATENCY RANGE. TRAJECTORIES OF ALL DRIVING MODELS ARE EVALUATED AGAINST THE LANE CENTER ACROSS VARIOUS SCENARIOS, INCLUDING FULL TRACK, STRAIGHT ROAD, LEFT TURN, AND RIGHT TURN.

Fig.14 ref.	Driving Model	Partial	Frechet	Area	Curve	Dynamic	DTSl↓
		Curve ↓	Distance ↓	Between ↓	Length ↓	Time ↓	
	Mapping		Curves		Warping		
(a) Full Track	BM, No Latency (ref)	1.19	2.176	4658.15	0.349	1253.21	0.034
(a) Full Track	BM, Latency = 0.0 – 0.35 sec	5.91	7.723	26498.2	1.245	4268.24	0.238
(a) Full Track	PLM-Net, Latency = 0.0 – 0.35 sec	2.547	3.616	29126.6	0.694	2653.26	0.028
(b) Straight	BM, No Latency (ref)	24.475	5.095	13.556	0.077	76.376	0.012
(b) Straight	BM, Latency = 0.0 – 0.35 sec	465.004	4.026	293.106	0.08	409.007	0.109
(b) Straight	PLM-Net, Latency = 0.0 – 0.35 sec	21.428	1.319	12.097	0.032	49.84	0.014
(c) Left turn	BM, No Latency (ref)	0.895	3.966	41.402	0.178	67.892	0.025
(c) Left turn	BM, Latency = 0.0 – 0.35 sec	1.697	4.449	209.537	0.284	198.209	0.107
(c) Left turn	PLM-Net, Latency = 0.0 – 0.35 sec	0.4	1.527	45.844	0.087	59.073	0.017
(d) Right turn	BM, No Latency (ref)	0.293	1.546	90.228	0.048	79.036	0.037
(d) Right turn	BM, Latency = 0.0 – 0.35 sec	0.744	4.572	420.415	0.11	228.825	0.097
(d) Right turn	PLM-Net, Latency = 0.0 – 0.35 sec	0.327	1.692	89.126	0.046	92.033	0.056

- [6] Z. Chen and X. Huang, "End-to-end learning for lane keeping of self-driving cars," in *Proc. IEEE Intell. Veh. Symp. (IV)*, 2017, pp. 1856–1860.
- [7] A. Khalil and J. Kwon, "Anec: Adaptive neural ensemble controller for mitigating latency problems in vision-based autonomous driving," in *2023 IEEE/RSJ International Conference on Intelligent Robots and Systems (IROS)*. IEEE, 2023, pp. 9340–9346.
- [8] F. Codevilla, M. Müller, A. López, V. Koltun, and A. Dosovitskiy, "End-to-end driving via conditional imitation learning," in *2018 IEEE International Conference on Robotics and Automation (ICRA)*, 2018, pp. 4693–4700.
- [9] D. D. Salvucci, "Modeling driver behavior in a cognitive architecture," *Human factors*, vol. 48, no. 2, pp. 362–380, 2006.
- [10] K. Berntorp, T. Hoang, R. Quirynen, and S. Di Cairano, "Control architecture design for autonomous vehicles," in *2018 IEEE Conference on Control Technology and Applications (CCTA)*. IEEE, 2018, pp. 404–411.
- [11] H. Lee, Y. Choi, T. Han, and K. Kim, "Probabilistically guaranteeing end-to-end latencies in autonomous vehicle computing systems," *IEEE Transactions on Computers*, 2022.
- [12] K. Strobel, S. Zhu, R. Chang, and S. Koppula, "Accurate, low-latency visual perception for autonomous racing: Challenges, mechanisms, and practical solutions," in *2020 IEEE/RSJ International Conference on Intelligent Robots and Systems (IROS)*. IEEE, 2020, pp. 1969–1975.
- [13] B. Vedder, J. Vinter, and M. Jonsson, "A low-cost model vehicle testbed with accurate positioning for autonomous driving," *Journal of Robotics*, vol. 2018, 2018.
- [14] X. Ge, "Ultra-reliable low-latency communications in autonomous vehicular networks," *IEEE Transactions on Vehicular Technology*, vol. 68, no. 5, pp. 5005–5016, 2019.
- [15] O. El Marai and T. Taleb, "Smooth and low latency video streaming for autonomous cars during handover," *Ieee Network*, vol. 34, no. 6, pp. 302–309, 2020.
- [16] S. R. Pokhrel, N. Kumar, and A. Walid, "Towards ultra reliable low latency multipath tcp for connected autonomous vehicles," *IEEE Transactions on Vehicular Technology*, vol. 70, no. 8, pp. 8175–8185, 2021.
- [17] Q. Zhang, H. Zhong, J. Cui, L. Ren, and W. Shi, "Ac4av: a flexible and dynamic access control framework for connected and autonomous vehicles," *IEEE Internet of Things Journal*, vol. 8, no. 3, pp. 1946–1958, 2020.
- [18] D. J. Gorsich, P. Jayakumar, M. P. Cole, C. M. Crean, A. Jain, and T. Ersal, "Evaluating mobility vs. latency in unmanned ground vehicles," *Journal of Terramechanics*, vol. 80, pp. 11–19, 2018.
- [19] I. Yaqoob, L. U. Khan, S. A. Kazmi, M. Imran, N. Guizani, and C. S. Hong, "Autonomous driving cars in smart cities: Recent advances, requirements, and challenges," *IEEE Network*, vol. 34, no. 1, pp. 174–181, 2019.
- [20] D. Pomerleau, "Alvinn: An autonomous land vehicle in a neural network," in *Proc. Adv. Neural Inf. Process. Syst.*, December 1989, pp. 305 – 313.
- [21] Net-Scale, "Autonomous Off-Road Vehicle Control Using End-to-End Learning," Jul. 2004. [Online]. Available: <http://net-scale.com/doc/net-scale-dave-report.pdf>
- [22] M. Bojarski *et al.*, "Explaining how a deep neural network trained with end-to-end learning steers a car," *arXiv preprint arXiv:1704.07911*, 2017. [Online]. Available: <http://arxiv.org/abs/1704.07911>
- [23] Q. Wang, L. Chen, B. Tian, W. Tian, L. Li, and D. Cao, "End-to-end autonomous driving: An angle branched network approach," *IEEE Trans. Veh. Technol.*, vol. 68, no. 12, pp. 11 599–11 610, 2019.
- [24] T. Wu, A. Luo, R. Huang, H. Cheng, and Y. Zhao, "End-to-end driving model for steering control of autonomous vehicles with future spatiotemporal features," in *Proc. IEEE/RSJ Int. Conf. Intell. Robots Syst.*, 2019, pp. 950–955.
- [25] J. Kwon, A. Khalil, D. Kim, and H. Nam, "Incremental end-to-end learning for lateral control in autonomous driving," *IEEE Access*, vol. 10, pp. 33 771–33 786, 2022.
- [26] T. Weiss and M. Behl, "Deepdracing: Parameterized trajectories for autonomous racing," *arXiv preprint arXiv:2005.05178*, 2020.
- [27] H. Mao, X. Yang, and W. J. Dally, "A delay metric for video object detection: What average precision fails to tell," in *Proceedings of the IEEE/CVF International Conference on Computer Vision*, 2019, pp. 573–582.
- [28] J. Kocić, N. Jovićić, and V. Drndarević, "An end-to-end deep neural network for autonomous driving designed for embedded automotive platforms," *Sensors*, vol. 19, no. 9, 2019. [Online]. Available: <https://www.mdpi.com/1424-8220/19/9/2064>
- [29] P. Wu, X. Jia, L. Chen, J. Yan, H. Li, and Y. Qiao, "Trajectory-guided control prediction for end-to-end autonomous driving: A simple yet strong baseline," *arXiv preprint arXiv:2206.08129*, 2022.
- [30] M. Bojarski, D. Del Testa, D. Dworakowski, B. Firner, B. Flepp, P. Goyal, L. D. Jackel, M. Monfort, U. Muller, J. Zhang *et al.*, "End to end learning for self-driving cars," *arXiv preprint arXiv:1604.07316*, 2016.
- [31] J. Kwon, "OSCAR (Open-Source robotic Car Architecture for Research and education)," Feb. 2021, original-date: 2020-11-29T19:48:57Z. [Online]. Available: <https://github.com/jrkwon/oscar>
- [32] M. Quigley, K. Conley, B. Gerkey, J. Faust, T. Foote, J. Leibs, R. Wheeler, A. Y. Ng *et al.*, "Ros: an open-source robot operating system," in *Proc. ICRA Workshop Open Source Softw.*, vol. 3, 2009, p. 5.
- [33] N. Koenig and A. Howard, "Design and use paradigms for gazebo, an open-source multi-robot simulator," in *2004 IEEE/RSJ International Conference on Intelligent Robots and Systems (IROS)(IEEE Cat. No. 04CH37566)*, vol. 3. IEEE, pp. 2149–2154.
- [34] C. F. Jekel, G. Venter, M. P. Venter, N. Stander, and R. T. Haftka, "Similarity measures for identifying material parameters from hysteresis loops using inverse analysis," *International Journal of Material Forming*, vol. 12, no. 3, pp. 355–378, 2019.
- [35] D. Kim, A. Khalil, H. Nam, and J. Kwon, "Opemi: Online performance evaluation metrics index for deep learning-based autonomous vehicles," *IEEE Access*, vol. 11, pp. 16 951–16 963, 2023.
- [36] D. P. Kingma and J. Ba, "Adam: A method for stochastic optimization," *arXiv preprint arXiv:1412.6980*, 2014.
- [37] A. Graves and A. Graves, "Long short-term memory," *Supervised sequence labelling with recurrent neural networks*, pp. 37–45, 2012.



Aws Khalil earned a B.S. in Mechatronics Engineering from the University of Jordan, Amman, Jordan in 2018. He received his M.S. degree from Budapest University of Technology and Economics (BME) in Autonomous Vehicle Control Engineering. He is currently a Ph.D. candidate in Electrical, Electronics, and Computer Engineering at the University of Michigan - Dearborn. Mr. Khalil is interested in autonomous vehicles, robotics, and deep learning. During his master's studies, he worked as a research assistant at BME Automated Drive Lab, and now he works at the University of Michigan - Dearborn's Bio-inspired Machine Intelligence (BIMI) Laboratory.



Jaerock Kwon (M'06–SM'20) received the B.S. and M.S. degrees from Hanyang University, Seoul, South Korea, in 1992 and 1994, respectively, and the Ph.D. degree in computer engineering from Texas A&M University, College Station, USA, in 2009. Between 1994 and 2004, he worked at LG Electronics, SK Teletech, and Qualcomm Internet Service. From 2009 to 2010, he was a Professor in the Department of Electrical and Computer Engineering at Kettering University, Flint, MI, USA. Since 2010, he has been a Professor in the Department of Electrical and Computer Engineering at the University of Michigan-Dearborn, MI, USA. His research interests include mobile robotics, autonomous vehicles, and artificial intelligence. Dr. Kwon's awards and honors include the Outstanding Researcher Award, Faculty Research Fellowship (Kettering University), and SK Excellent Employee (SK Teletech). He served as the President of the Korean Computer Scientists and Engineers Association in America (KOCSEA) in 2020 and 2021.

APPENDIX A

CONSTANT PERCEPTION LATENCY

The following are the results from the different constant *perception latency* values that we tested to validate our model *PLM-Net*. The interpretation of these results is similar to that in Section V, so directly show the relevant figures and tables for each latency value.

A. Perception Latency 0.15 seconds

This subsection illustrates the results when the perception latency was 0.15 seconds. Fig.15 and Table VII shows the steering comparison against time. Fig.16 compares driving trajectories colored based on steering angle values. Fig.21 and Table X shows the trajectory similarity.

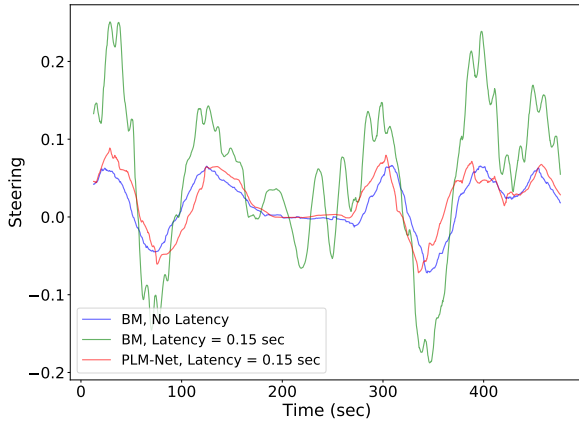


Fig. 15. Qualitative comparison of steering angle over time. The blue line represent the *BM* driving on the test track with no latency. The green line represent the *BM* driving on the test track with 0.15 seconds latency. The red line the *PLM-Net* driving on the test track with the same latency value.

TABLE VII

STEERING ANGLE ERROR METRICS. COMPARISON OF STEERING ANGLE ERROR BETWEEN *BM* DRIVING WITHOUT LATENCY, *BM* DRIVING WITH LATENCY OF 0.15 SECONDS, AND *PLM-Net* DRIVING WITH THE SAME LATENCY

<i>BM, No latency vs.</i>	<i>MAE</i> ↓	<i>MSE</i> ↓	<i>RMSE</i> ↓
<i>BM, Latency = 0.15 sec</i>	0.171355	0.0570811	0.238916
<i>PLM-Net, Latency = 0.15 sec</i>	0.053122	0.00691402	0.0831506

B. Perception Latency 0.25 seconds

This subsection illustrates the results when the perception latency was 0.25 seconds. Fig.17 and Table VIII shows the steering comparison against time. Fig.18 compares driving trajectories colored based on steering angle values. Fig.22 and Table XI shows the trajectory similarity.

C. Perception Latency 0.30 seconds

This subsection illustrates the results when the perception latency was 0.30 seconds. Fig.19 and Table IX shows the steering comparison against time. Fig.20 compares driving trajectories colored based on steering angle values. Fig.23 and Table XII shows the trajectory similarity.

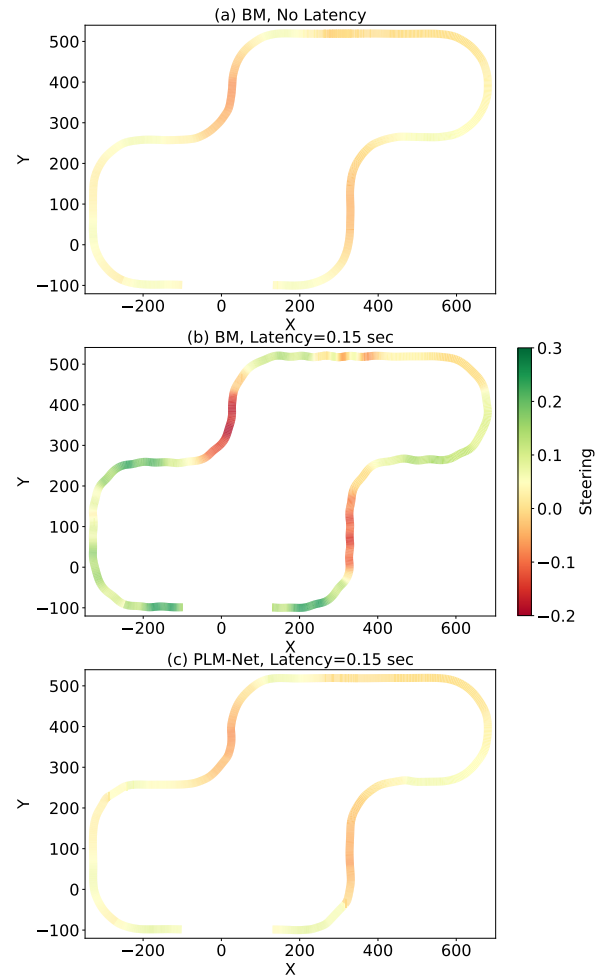


Fig. 16. Vehicle trajectories colored by steering angle. (a) The trajectory of the *BM* driving with no latency. (b) The trajectory of the *BM* driving with 0.15 seconds latency. (c) The trajectory of the *PLM-Net* driving with 0.15 seconds latency.

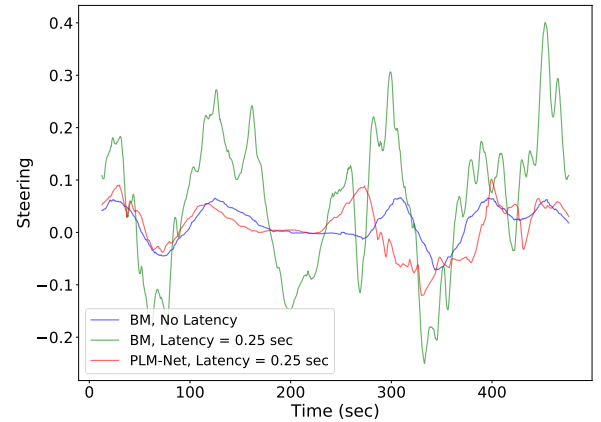


Fig. 17. Qualitative comparison of steering angle over time. The blue line represent the *BM* driving on the test track with no latency. The green line represent the *BM* driving on the test track with 0.25 seconds latency. The red line the *PLM-Net* driving on the test track with the same latency value.

APPENDIX B

TRAINING RESULTS

Fig.24 shows the training results for the *PLM-Net* models. Each sub-figure shows the predicted vs ground truth steering

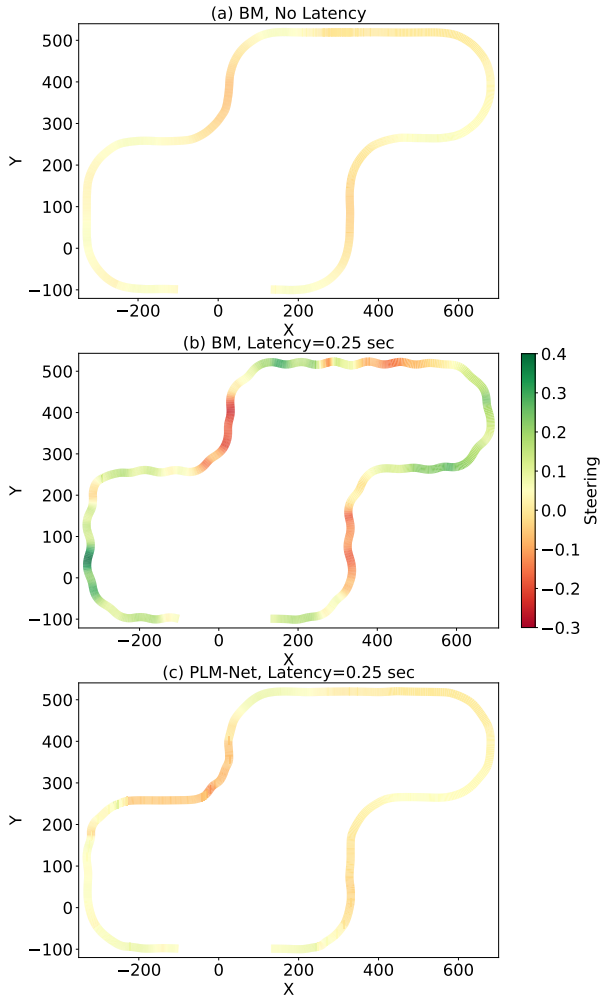


Fig. 18. Vehicle trajectories colored by steering angle. (a) The trajectory of the *BM* driving with no latency. (b) The trajectory of the *BM* driving with 0.25 seconds latency. (c) The trajectory of the *PLM-Net* driving with 0.25 seconds latency.

TABLE VIII

STEERING ANGLE ERROR METRICS. COMPARISON OF STEERING ANGLE ERROR BETWEEN *BM* DRIVING WITHOUT LATENCY, *BM* DRIVING WITH LATENCY OF 0.25 SECONDS, AND *PLM-Net* DRIVING WITH THE SAME LATENCY

<i>BM</i> , No latency vs.	MAE ↓	MSE ↓	RMSE ↓
<i>BM</i> , Latency = 0.25 sec	0.334727	0.18581	0.431057
<i>PLM-Net</i> , Latency = 0.25 sec	0.0921437	0.0192333	0.138684

TABLE IX

STEERING ANGLE ERROR METRICS. COMPARISON OF STEERING ANGLE ERROR BETWEEN *BM* DRIVING WITHOUT LATENCY, *BM* DRIVING WITH LATENCY OF 0.3 SECONDS, AND *PLM-Net* DRIVING WITH THE SAME LATENCY

<i>BM</i> , No latency vs.	MAE ↓	MSE ↓	RMSE ↓
<i>BM</i> , Latency = 0.3 sec	0.226148	0.0968093	0.311142
<i>PLM-Net</i> , Latency = 0.3 sec	0.0710674	0.0107641	0.10375

angle. Fig.24(a) *BM* training results where $\delta_{ref} = 0.0$.

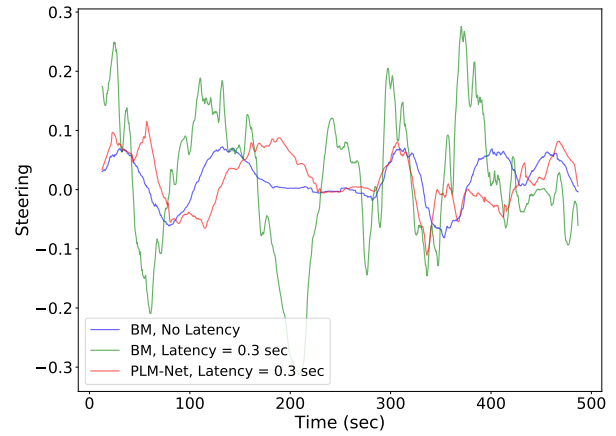


Fig. 19. Qualitative comparison of steering angle over time. The blue line represent the *BM* driving on the test track with no latency. The green line represent the *BM* driving on the test track with 0.3 seconds latency. The red line the *PLM-Net* driving on the test track with the same latency value.

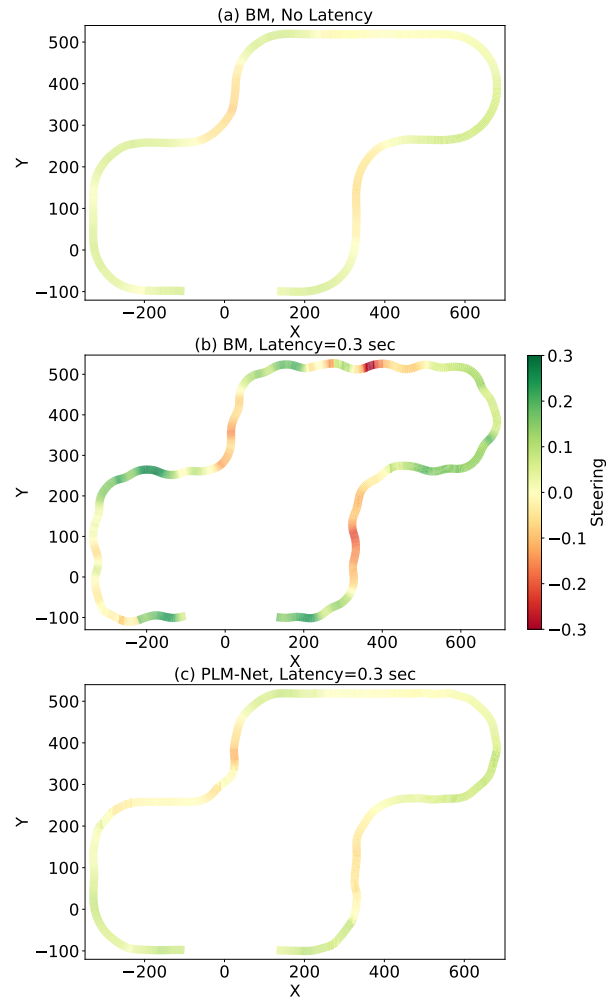


Fig. 20. Vehicle trajectories colored by steering angle. (a) The trajectory of the *BM* driving with no latency. (b) The trajectory of the *BM* driving with 0.3 seconds latency. (c) The trajectory of the *PLM-Net* driving with 0.3 seconds latency.

Fig. 24(b)-(f) *TAPM* training results for all other values of δ_{ref} , as the *TAPM* predicts five future steering angles.

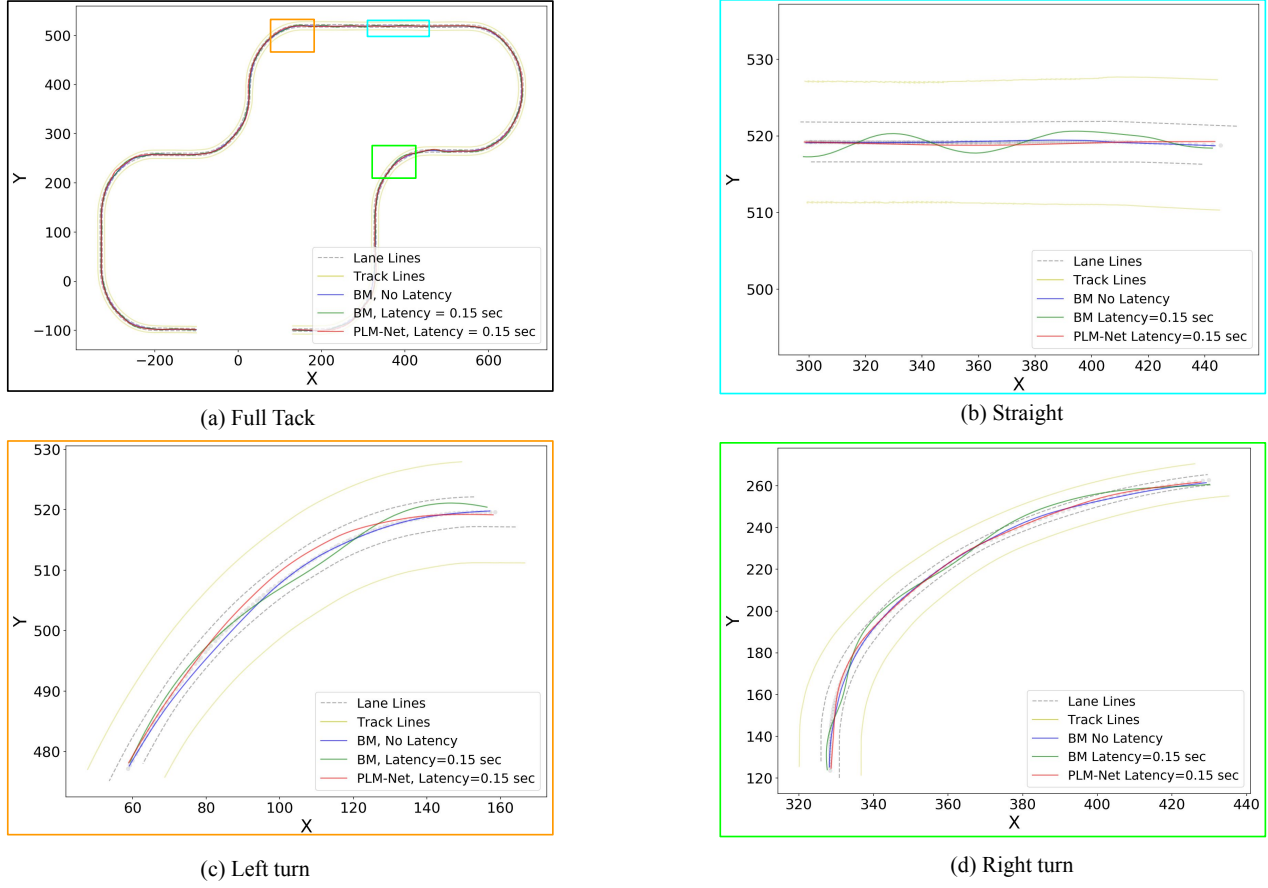


Fig. 21. Trajectory comparison between: The *BM* driving with no latency (blue line), the *BM* driving with with 0.15 seconds latency (green line), and the *PLM-Net* driving with 0.15 seconds latency (red line). (a) The trajectories on the full test track. (b) The trajectories on a straight road segment. (c) The trajectories on a left turn. (d) The trajectories on a right turn.

TABLE X
 QUANTITATIVE COMPARISON OF DRIVING TRAJECTORY SIMILARITY, BETWEEN *BM* DRIVING WITHOUT LATENCY, *BM* DRIVING WITH LATENCY OF 0.15 SECONDS, AND *PLM-Net* DRIVING WITH THE SAME LATENCY. ALL DRIVING MODELS' TRAJECTORIES ARE COMPARED WITH THE LANE CENTER ON FULL TRACK, STRAIGHT ROAD, LEFT TURN, AND RIGHT TURN.

Fig.21 ref.	Driving Model	Partial	Frechet	Area	Curve	Dynamic	DTSL \downarrow
		Curve \downarrow Mapping	Distance \downarrow	Between \downarrow Curves	Length \downarrow	Time \downarrow Warping	
(a) Full Track	BM, No Latency (ref)	1.19	2.176	4658.15	0.349	1253.21	0.034
(a) Full Track	BM, Latency = 0.15 sec	1.931	4.087	15946.7	0.432	2343.73	0.266
(a) Full Track	PLM-Net, Latency = 0.15 sec	1.579	4.543	13035	0.383	2255.83	0.041
(b) Straight	BM, No Latency (ref)	24.475	5.095	13.556	0.077	76.376	0.012
(b) Straight	BM, Latency = 0.15 sec	229.411	5.918	123.118	0.109	213.709	0.016
(b) Straight	PLM-Net, Latency = 0.15 sec	63.767	5.566	34.741	0.086	97.41	0.012
(c) Left turn	BM, No Latency (ref)	0.895	3.966	41.402	0.178	67.892	0.025
(c) Left turn	BM, Latency = 0.15 sec	0.932	4.115	98.63	0.179	113.299	0.07
(c) Left turn	PLM-Net, Latency = 0.15 sec	0.531	2.126	81.367	0.141	92.124	0.058
(d) Right turn	BM, No Latency (ref)	0.293	1.546	90.228	0.048	79.036	0.037
(d) Right turn	BM, Latency = 0.15 sec	0.746	3.971	285.641	0.08	169.875	0.113
(d) Right turn	PLM-Net, Latency = 0.15 sec	0.313	1.882	67.192	0.05	75.371	0.098

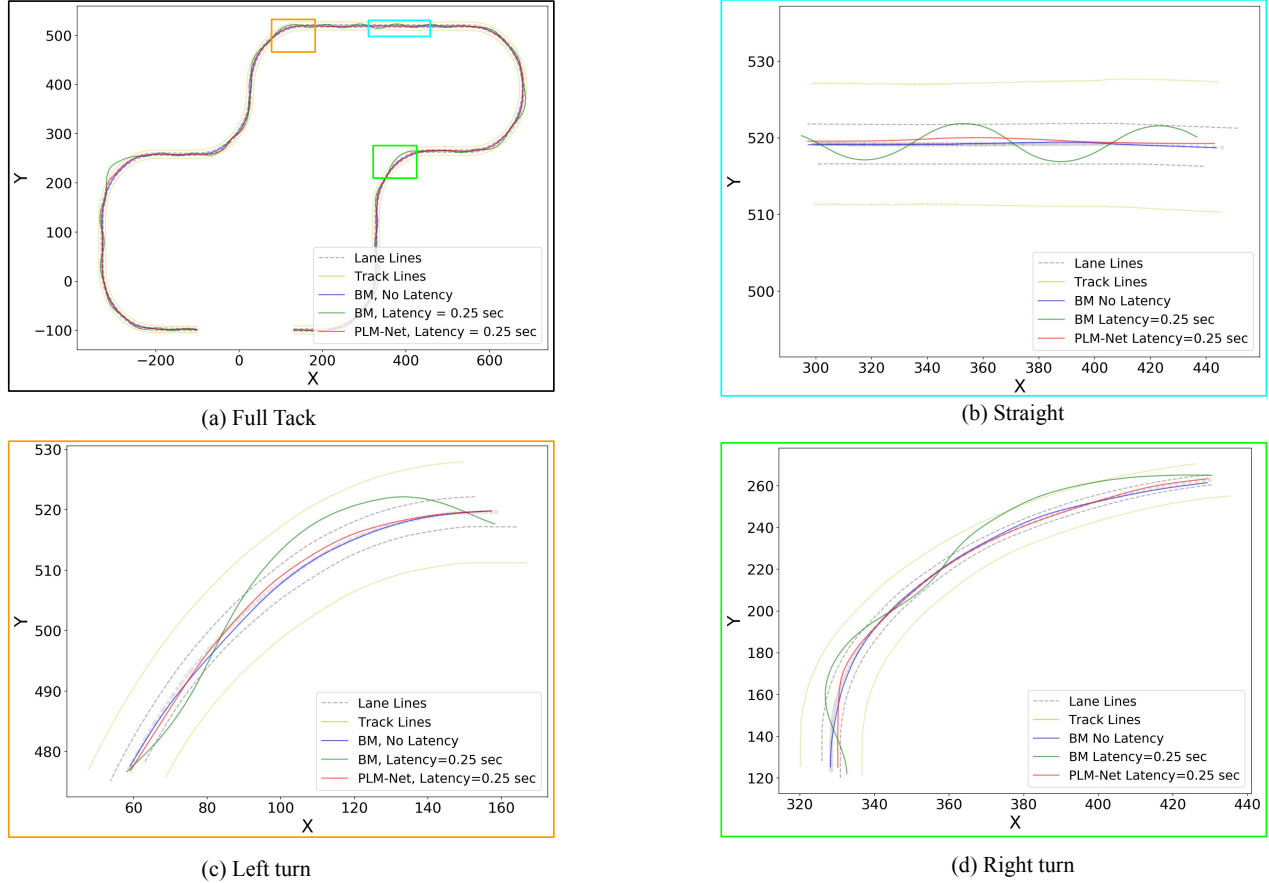


Fig. 22. Trajectory comparison between: The *BM* driving with no latency (blue line), the *BM* driving with 0.25 seconds latency (green line), and the *PLM-Net* driving with 0.25 seconds latency (red line). (a) The trajectories on the full test track. (b) The trajectories on a straight road segment. (c) The trajectories on a left turn. (d) The trajectories on a right turn.

TABLE XI

QUANTITATIVE COMPARISON OF DRIVING TRAJECTORY SIMILARITY, BETWEEN *BM* DRIVING WITHOUT LATENCY, *BM* DRIVING WITH LATENCY OF 0.25 SECONDS, AND *PLM-Net* DRIVING WITH THE SAME LATENCY. ALL DRIVING MODELS' TRAJECTORIES ARE COMPARED WITH THE LANE CENTER ON FULL TRACK, STRAIGHT ROAD, LEFT TURN, AND RIGHT TURN.

Fig.22 ref.	Driving Model	Partial	Frechet	Area	Curve	Dynamic	DTSI \downarrow
		Curve \downarrow	Distance \downarrow	Between \downarrow	Length \downarrow	Time \downarrow	
		Mapping	Curves			Warping	
(a) Full Track	BM, No Latency (ref)	1.19	2.176	4658.15	0.349	1253.21	0.034
(a) Full Track	BM, Latency = 0.25 sec	8.077	18.917	25958.2	2.09	7459.15	0.36
(a) Full Track	PLM-Net, Latency = 0.25 sec	3.47	5.357	91195.1	0.814	3637.4	0.046
(b) Straight	BM, No Latency (ref)	24.475	5.095	13.556	0.077	76.376	0.012
(b) Straight	BM, Latency = 0.25 sec	680.624	4.756	359.311	0.122	550.559	0.077
(b) Straight	PLM-Net, Latency = 0.25 sec	150.696	3.053	78.985	0.072	122.401	0.046
(c) Left turn	BM, No Latency (ref)	0.895	3.966	41.402	0.178	67.892	0.025
(c) Left turn	BM, Latency = 0.25 sec	2.999	5.542	349.446	0.156	326.643	0.13
(c) Left turn	PLM-Net, Latency = 0.25 sec	0.973	4.765	61.525	0.218	89.88	0.093
(d) Right turn	BM, No Latency (ref)	0.293	1.546	90.228	0.048	79.036	0.037
(d) Right turn	BM, Latency = 0.25 sec	1.79	9.468	810.979	0.222	438.145	0.11
(d) Right turn	PLM-Net, Latency = 0.25 sec	0.199	1.971	108.645	0.032	103.168	0.065

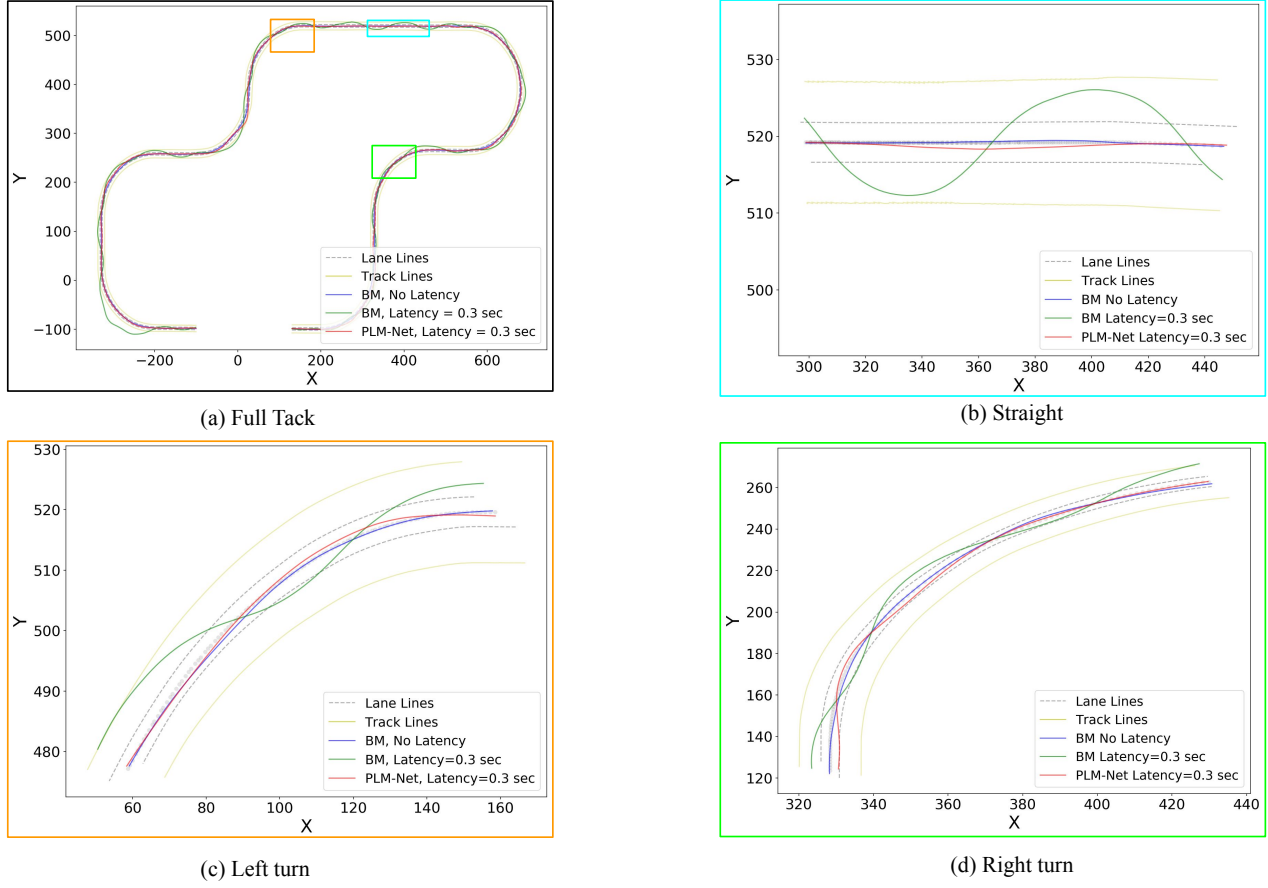


Fig. 23. Trajectory comparison between: The *BM* driving with no latency (blue line), the *BM* driving with with 0.3 seconds latency (green line), and the *PLM-Net* driving with 0.3 seconds latency (red line). (a) The trajectories on the full test track. (b) The trajectories on a straight road segment. (c) The trajectories on a left turn. (d) The trajectories on a right turn.

TABLE XII
QUANTITATIVE COMPARISON OF DRIVING TRAJECTORY SIMILARITY, BETWEEN *BM* DRIVING WITHOUT LATENCY, *BM* DRIVING WITH LATENCY OF 0.3 SECONDS, AND *PLM-Net* DRIVING WITH THE SAME LATENCY. ALL DRIVING MODELS' TRAJECTORIES ARE COMPARED WITH THE LANE CENTER ON FULL TRACK, STRAIGHT ROAD, LEFT TURN, AND RIGHT TURN.

Fig.23 ref.	Driving Model	Partial	Frechet	Area	Curve	Dynamic	DTSI
		Curve ↓	Distance ↓	Between ↓	Length ↓	Time ↓	↓
		Mapping		Curves		Warping	
(a) Full Track	BM, No Latency (ref)	1.19	2.176	4658.15	0.349	1253.21	0.034
(a) Full Track	BM, Latency = 0.3 sec	16.097	28.429	93980.4	4.494	15235.3	0.391
(a) Full Track	PLM-Net, Latency = 0.3 sec	2.189	7.033	80617.1	0.606	3524.91	0.02
(b) Straight	BM, No Latency (ref)	24.475	5.095	13.556	0.077	76.376	0.012
(b) Straight	BM, Latency = 0.3 sec	1046.2	7.968	631.198	0.203	911.435	0.192
(b) Straight	PLM-Net, Latency = 0.3 sec	97.525	6.002	59.361	0.108	117.782	0.014
(c) Left turn	BM, No Latency (ref)	0.895	3.966	41.402	0.178	67.892	0.025
(c) Left turn	BM, Latency = 0.3 sec	3.088	8.825	422.69	0.556	398.425	0.161
(c) Left turn	PLM-Net, Latency = 0.3 sec	0.514	1.047	60.492	0.019	69.811	0.034
(d) Right turn	BM, No Latency (ref)	0.293	1.546	90.228	0.048	79.036	0.037
(d) Right turn	BM, Latency = 0.3 sec	1.235	9.1	1321.13	0.2	545.015	0.482
(d) Right turn	PLM-Net, Latency = 0.3 sec	0.21	2.529	162.868	0.039	120.484	0.148

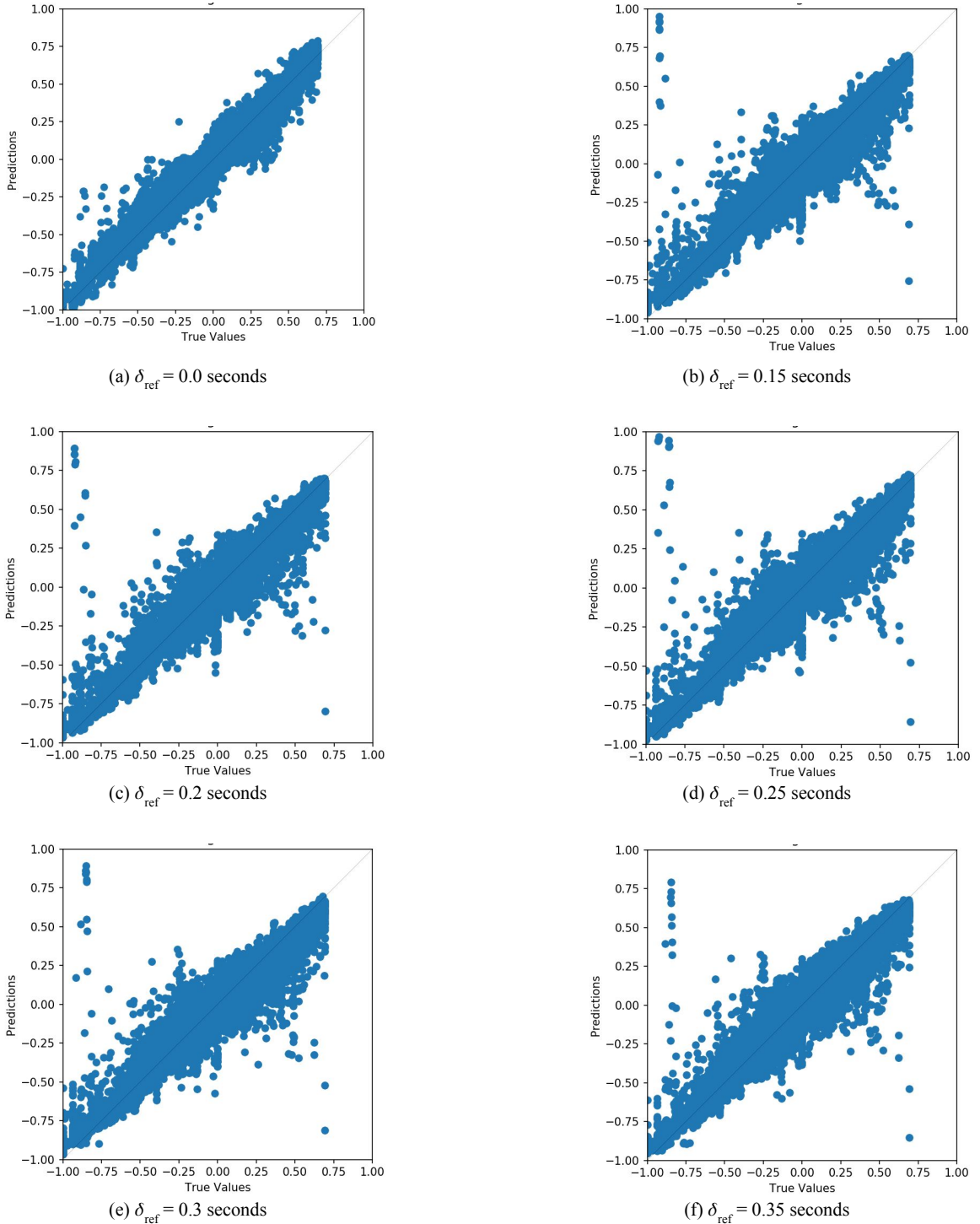


Fig. 24. *PLM-Net* models training results. Each sub-figure shows the predicted vs ground truth steering angle. (a) *BM* training results where $\delta_{ref} = 0.0$. (b)-(f) *TAPM* training results for all other values of δ_{ref} , as the *TAPM* predicts five future steering angles.